Arabian Journal of Chemistry (2021) **14**, 103367

King Saud University

Arabian Journal of Chemistry

www.ksu.edu.sa
www.sciencedirect.com

ORIGINAL ARTICLE

Multi-functional epoxy composite coating incorporating mixed Cu(II) and Zr(IV) complexes of metformin and 2,2\-bipyridine as intensive network cross-linkers exhibiting anti-corrosion, self-healing and chemical-resistance performances for steel petroleum platforms

A.M. Fadl [a,*], S.A. Sadeek [b], Laila Magdy [b], M.I. Abdou [a], W.H. El-Shiwiniy [b,c]

[a] *Production Department, Egyptian Petroleum Research Institute, Nasr City, Cairo, Egypt*
[b] *Department of Chemistry, Faculty of Science, Zagazig University, 44519 Zagazig, Egypt*
[c] *Department of Chemistry, College of Science, Bisha University, Bisha, Saudi Arabia*

Received 22 June 2021; accepted 28 July 2021
Available online 02 August 2021

KEYWORDS

Cu(II) and Zr(IV) complex cross-linkers;
Anti-corrosion behavior;
Effective magnetic moment;
Distorted octahedral geometry;
Chemical resistance;
AFM

Abstract Metal-organic network cross-linking agents are commingled with epoxy for establishing multi-functional coating system with robust resistance properties for steel protection applications in harsh atmospheres. To support this concept, the present study relates to fabrication of new mixed ligand Cu(II) and Zr(IV) complexes of metformin (MF) and 2.2′bipyridine (bpy) as coating surface cross-linking modifiers to guard the steel surface of petroleum platforms from corrosion in severe environments. CHN analysis, molar conductance, magnetic susceptibility, FT-IR, UV–Visible, ^{1}H NMR and TGA/DTG analysis were performed for full characterizations of the two ligands and their mixed complexes. The elemental analysis data affirmed the chemical formula of the formed complexes. Molar conductance measurements proved that the complexes were electrolytic in nature with 1:2 (metal:ligand) molar ratio. The FT-IR analysis for MF, bpy and their complexes manifested that MF and bpy chelated with metal ions as bidentate ligands through two imines (-C = NH) groups in MF and through two nitrogen of pyridine rings in bpy. The TGA/DTG analysis demonstrated the thermal stability and decomposition of the complexes. The magnetic moment measurements offered paramagnetic properties for Cu(II), μ_{eff} = 1.70 B.M. The structure geometry

* Corresponding author.
E-mail address: fadl8693@yahoo.com (A.M. Fadl).
Peer review under responsibility of King Saud University.

Production and hosting by Elsevier

https://doi.org/10.1016/j.arabjc.2021.103367

survey affirmed a distorted octahedral geometry of the formed Cu(II) and Zr(IV) complexes. Epoxy coating formulations loaded with the same concentration of MF, bpy, Cu(II), and Zr(IV) compounds were applied and evaluated. Salt spray corrosion trial demonstrated that PA-DGEBA/MC-Cu coating achieved advanced corrosion mitigation demeanor at blistering size of #8, few frequency and calculated rust grade at 10. SEM morphology and EDX analysis were performed to explicate the protective performance in which PA-DGEBA/MC-Cu coated layer displayed the least Fe peak count at 2.5 without appearance of rusting. AFM microstructure of surface-modified Cu(II) epoxy coating offered the most smooth surface (Ra = 1.78 nm, Rq = 2.99 nm), with a harder matrix and perfect nonporous coating surface. Acid spot test checked the chemical resistance of these coatings and elucidated that DGEBA/MC-Cu coating achieved the highest acid resistances at Level 0 by H_2SO_4 (96%), HNO_3 (70%) and HCl (37%) against full deterioration of blank neat epoxy at Level 3.

1. Introduction

More than 23% of the world's oil and gas production is from offshore wells accounted roughly by 17,000 wells. Steel offshore platforms are constructed for the petroleum production in the severe aggressive sea water environment (Olajire, 2017; https://www.pcimag.com/articles/, 2019; Schremp, 1984). Oil and gas offshore platforms are large drilling rigs used for exploring, extraction, storing, and processing petroleum and natural gas that located in rock formations under the seabed and the most famous types are the fixed platforms (https://www.pcimag.com/articles/, 2019). Protective maintenance for offshore platforms against corrosive marine surroundings is required by using modified splash zone preventative epoxy coatings (Schremp, 1984). Prophylactic epoxy coatings were used for surface protection of different steel structures due to their superb anti-corrosion demeanor, high bonding properties, chemical immovability, and strong ascendant mechanical resistance (Ramezanzadeh et al., 2019; Fadl et al., 2020; Ashassi-Sorkhabi et al., 2016). In addition to having good thermal and mechanical properties as a thermosetting polymer, epoxy coating offers strong adhesion intact with the metal substrate and has low curing shrinkage at room temperature environment (Gibson and Resins, 2017). However, poor barrier property against the attack by caustic agents is a highly influential drawback of epoxy coating. An epoxy coating usually offered some blistering and wrinkling problems and interfacial adhesive bond breakage owing to the diffusion of the aggressive species to spread via zigzag open sites upon the coating/metal interface, thereby accelerating the degradation of epoxy coating after prolonged exposure (Yue, 2020; Pourhashem et al., 2017). Despite these disadvantages, the investigation on epoxy-based protective coating is still progressing and many pieces of research have reported the modification of epoxy polymeric systems to improve the protection ability (Qiu et al., 2017; Pourhashem et al., 2017; Ganjaee and Ramezanzadeh, 2020). Consequently, advanced multifunctional epoxy system for protecting the steel walls of offshore platforms from the harsh outdoor conditions is believed to be an indispensable topic for successful petroleum production.

Metformin (MF) as illustrated in Scheme 1a displayed conspicuous coordinative and biological properties (Vasantha et al., 2018; Shahabadi and Heidari, 2012). MF reacted with some aldehyde derivatives forming Schiff base compounds which reacted with some metal ions forming metal complexes (Mahmoud et al., 2019; El-Shwiniy et al., 2020). Evaluating the biological behavior of certain complexes depended on investigating the interaction of them with glucose in phosphate buffer solution and the data were indicated by a robust binding connection between glucose and complexes at pH 7.4 (aqueous medium) (Mahmoud et al., 2019; El-Shwiniy et al., 2020). MF is utilized as an ideal curing for type II diabetes, and can be used as an analgesic, antimicrobial, antimalarial (Zhu et al., 2002). 2;2\-Bipyridine (bpy) is an hetero organic compound as shown in Scheme 1b. Recently, bpy became a wide spread ligand in both macromolecular and supramolecular chemistry (Schubert and Eschbaumer, 2002; Kaes et al., 2000). The bpy demonstrated a valuable electrochemical demeanor, variable photo-optical, photo-physical properties and reacted with metal ions by the two nitrogen of pyridine aromatic rings (Elsevier et al., 2003; Solovyev et al., 2018; Abd El-Hamid et al., 2017). Metal complexes can be more active than their free ligands, especially those having N-donor heterocyclic which chelate to the metal ion (Dendrinou-Samara et al., 2001; Efthimiadou et al., 2007).

Several studies investigated the preparation of p-Phenyla mine-N(4-chlorosalicylaldenemine) Schiff base ligand and its metal complexes to evaluate their corrosion mitigation behavior and chemical durability via the epoxy/SiO_2 nanocomposite coating surface applied on C-steel substrate (Fadl et al., 2020). The obtained results affirmed the prominent protective performance of Ni(II) and Cr(III) complexes via the coating film. Furthermore, the mechanical properties of these designed coatings were improved owing to their elevated magnetic dipole moment and electronegativity values in which enhanced the donor–acceptor interactions via steel/coating interface, thereby enhancing the cross-linking intensity and reinforcing the chemical bonding and interfacial adhesion (Fadl et al., 2019).

Fabrication of transition metal containing polyhedral oligomeric silsesquioxane complexes was carried out from octa carboxyl polyhedral oligomeric silsesquioxane (OC-POSS) and blended with epoxy coating system (Zhang et al., 2021). The obtained results showed that the remaining carboxyl groups of M@POSS-COOH that could react with epoxy groups along with the mesoporous structure increased the network strength of the epoxy resin (EP), and played a significant role in improving the mechanical, dielectric and thermal prop-

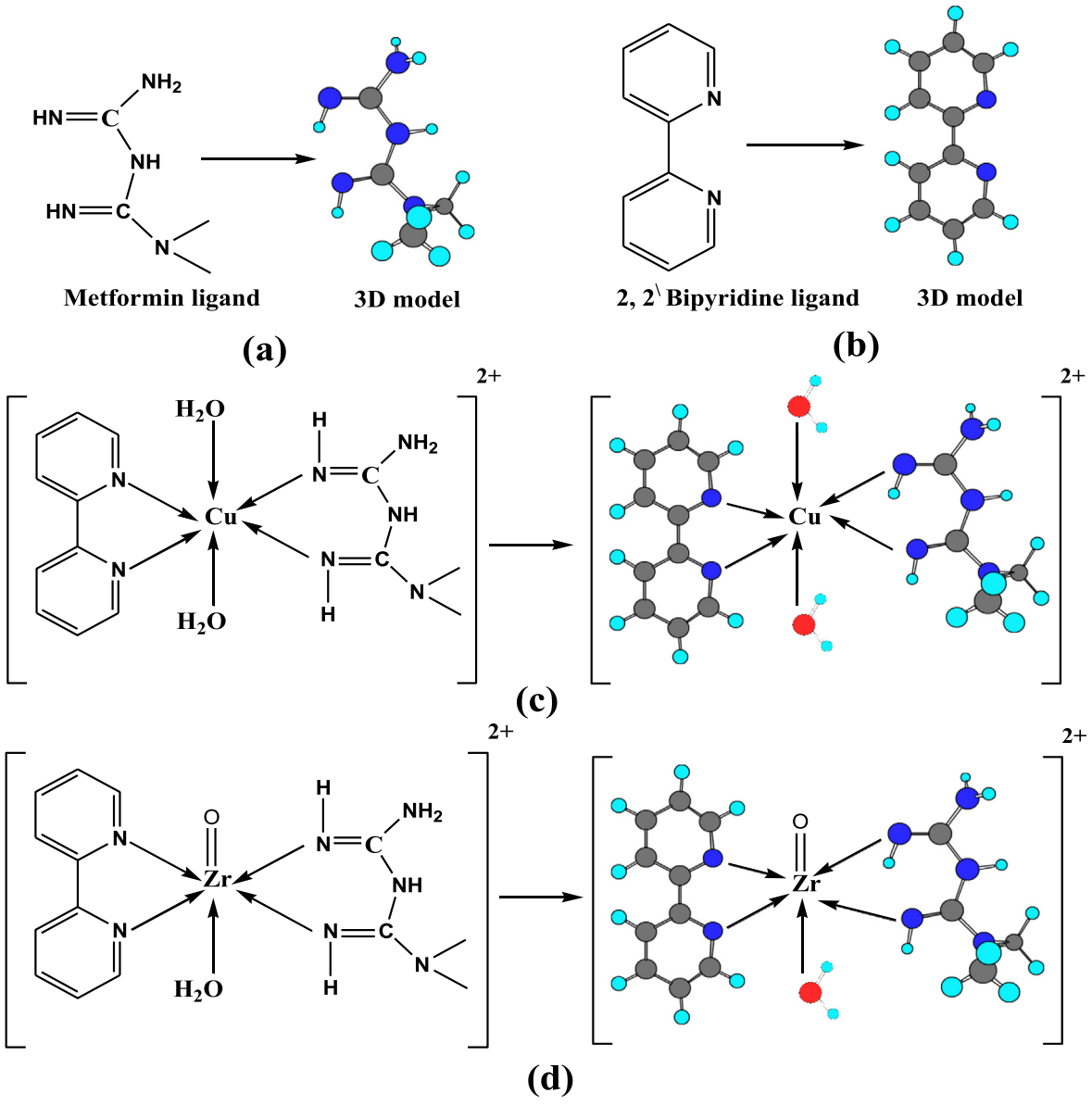

Scheme 1 Structure of (a) MF, (b) bpy, (c) Cu(II) complex and (d) Zr(IV) complex and their 3D models.

erties of the composites. As reported before in the published literature, Mn(II) complexes were fabricated and identified as drying agents for the alkyd coating layer as alternative to Co (II) driers (Lalgudi et al., 2009). Aluminum complex such as tris(8 -hydroxyquinoline), aluminum salt was prepared and characterized as drier and cross-linker for alkyd vehicles (Harrington et al., 2010). Super-functional dopa–iron complexes and tannic acid Fe(III) complexes acted by continuous deposition were fabricated and evaluated on solid substrates (Ejima et al., 2013; Li et al., 2016). Furthermore, some phytic acid-Co(II) and Ni(II) complex coatings were precipitated by immersing the steel films in a solution composed of metal ions and the employed acid to offer superb corrosion mitigation behavior on steel surface (Yan et al., 2017).

The present study investigates the synthesis, characterization and density functional theory (DFT) studies of novel fabricated mixed ligand Cu(II), and Zr(IV) complexes of MF and bpy ligands. These complexes are described using elemental, magnetic moment, molar conductance, (TGA/DTG), FT-IR, UV–Vis. and ^{1}H NMR analysis. Detection for the delicate structure of the investigated complex compounds in addition to calculating the total dipole moment, total energy and heat of formation are made using DFT measurements. Furthermore, the anticorrosion and acid resistance properties of epoxy coating modified with the same concentration of these metal complexes and their free ligands are discussed using the international standard coating evaluation tests to assert their application efficiency.

2. Experimental

2.1. Materials and instruments

The present investigation employed chemicals with pure grade of ($CuCl_2{\cdot}2H_2O$, $ZrOCl_2{\cdot}8H_2O$, MF, bpy and acetone), deliv-

ered from BDH, Aldrich or Sigma. Polyamine hardener (Ancamine curing agent1734) consists of DDM (4,4′-diaminodiphenyl methane), was obtained from Anchor Chemicals. BECKOPOX™ EP 128 (solvent-free liquid epoxy resin), was delivered from Allnex coating resins Company, Germany. Isopropyl alcohol, ethylene glycol, isobutanol and xylene were acquired by El-Mohandes Company for solvents and chemicals, Egypt·THF was conducted from Palmer Holland, Inc. Chromaflo Technologies Company was the source of Dioctyl phithalate (D.O.P). Obtaining of anhydrous 99.9% of dimethyl sulfoxide (DMSO), was made by Sigma Aldrich Company. The steel films were provided with 5 cm × 10 cm × 2 mm × dimensions for the salt spray trial. Steel pieces utilized for the cure chemical durability evaluation were with dimensions of 15 cm × 10 cm × 0.8 mm. The C-steel panels used for surface morphology and microstructure surveys were prepared with dimensions of 1 cm × 1 cm × 0.8 m m. Surface roughness around 50 μm was obtained by sand-blasting machine. Then, washing by acetone and distilled water was carried out for coating to be ready applied **(ASTM D 609–00)**. The XRF chemical analysis of steel surface underlined its composition as : Al 0.023%, C 0.090%, Mn 1.440%, P 0.190%, Cr 0.590%, Ni 0.220%, Si 0.437%, Cu 0.150 %, Mo 0.050%, V + Ti 0.020% and Fe represented the Balance.

Perkin Elmer 2400 CHN elemental analyzer was utilized for elemental analysis. The atomic absorption method was made using Spectrometer model PYE-UNICAM SP 1900 for detecting gravimetrically the percent of metal ions. FT-IR 460 PLUS Spectrophotometer was utilized to detect FT-IR spectra using KBr discs in 4000–400 cm^{-1} range. Varian Mercury VX-300 NMR Spectrometer was utilized for recording ^1H NMR spectra incorporating DMSO d_6 solvent. TGA-50H Shimadzu was utilized to measure TGA-DTG and implemented at temperature range of 25–1000 under N_2 atmosphere ^oC, and an alumina crucible was used for accurate sample weighting. UV-3101PC Shimadzu was employed for detecting the electronic spectra. Recording the absorption spectra as solutions was made in DMSO d_6 solvent. Sherwood scientific magnetic balance was anticipated at room temperature to measure the magnetic susceptibilities of the solid powdered samples utilizing Gouy balance at 25 ^oC, with using calibrant (Hg[Co(SCN)$_4$]). CONSORT K410 was utilized for measuring the molar conductance of the MF and BiPy and their complexes at concentration 1 × 10^{-3} M of solutions in DMSO. Buchi apparatus was employed for recording the melting points of the investigated compounds. Scanning electron microscopic (SEM) micrographs of the coated panels were illustrated by SEM apparatus (QUANTA FEG 250) with magnification of 800 X to offer the morphology of the applied coating surfaces after the immediate exposure to the aggressive environment. EDX appliance connected with SEM device (QUANTA FEG 250) was employed to underline the modification process of the investigated coatings with ligands and their mixed metal complexes. AFM analysis was made using a Shimadzu SPM-9600 microscope with minimum resolution of 400 nm.

2.2. Fabrication of the employed mixed complexes

The dark blue solid complex $[Cu(MF)(bpy)(H_2O)_2]Cl_2{\cdot}2H_2O$ was synthesized by mixing 1 mmol (0.165 g) of MF in 40 ml of acetone and 1 mmol (0.156 g) of bpy with the same ratio of 1 mmol of $CuCl_2{\cdot}2H_2O$ Refluxing for the mixture was made and a precipitate with dark blue color was obtained and dried over anhydrous $CaCl_2$ under vacuum. The pink solid complex $[ZrO(MF)(bpy)H_2O]Cl_2$ was fabricated similarly as sketched above utilizing acetone solvent and $ZrOCl_2$ś$8H_2O$, in 1:1:1 (M^{n+}: MF: bpy) molar ratios. Unfortunately we were not able to obtained appropriate mono-crystals to perform X-ray crystallographic measurements after applied several techniques such as crystallization by slow evaporation and cooling. In absence of X-ray crystallographic study, we enhance the technical quality of the manuscript by quantum chemical calculation.

2.3. DFT computational specifics

Extremely delicate measurements including the parameters of geometry, energies and atomic charges for MF, bpy, Cu(II), and Zr(IV) compounds were determined and figured by DFT (Frisch, 1998) along with the B3LYP functional (Kohn and Sham, 1965; Becke, 1988) and Lee, Yange Parrs (Lee et al., 1988), together with the Hartree-Fock local exchange function (Flurry, 1968).

2.4. Coating modification with MF, bpy and their complexes

MF and bpy and their as-prepared mixed Cu(II), and Zr(IV) complexes (0.1 g, wt) were dissolved separately in mixed solvents (50 ml) in ratio by weight (20 isobutanol: 30 THF: 50 DMSO) for 20 min using ultrasonic device. Then, heating of the mixture was carried out for full dissolving of the undissolved parts of MF, bpy and their mixed complexes to prepare the ionic solutions of them. By using ultra-sonic devices with robust stirring for 30 min, 1% of the prepared ionic lotions were added separately to the epoxy resin using xylene for obtaining identical hybrid epoxy coating formulations (PA-DGEBA/MF, PA-DGEBA/bpy, PA-DGEBA/MC-Cu, and PA-DGEBA/MC-Zr), against neat epoxy (blank unmodified conventional coating). The investigated hardener used for curing the employed coatings was 4,4′-diaminodiphenyl methane (Ancamine 1734), and added to epoxy in (0.6:1) ratios and the dry coating layer thickness, DFT was measured in range of 70 ± 5 μm using magnetic gauge.

2.5. Corrosion trial (Salt spray test)

Salt spray trial utilizing Sheen chamber as a closed model was implemented for corrosion inhibiting evaluation of the investigated compounds through the coating film. The cabinet conditions including; saline sodium chloride solution, 95% humidity with applied temperature of 35 ^oC. According to **ASTM B117-03**, X-shaped cross-lines were made using sharp cutter via the coating films for corrosive fog permeation and reaching C-steel surface via this scratched zone of the coating and the coated films were established in the parallel plates of the chamber during performing the test. Evaluating the corrosion mitigation of these coated layers on the steel surface was made using the international standards; **API 5L2 4th edition, July 2002** (softening grade), **ASTM D 3359–97,** (adhesion degree), **ASTM D 714–02** (frequency and size of blistering), and **ASTM D 810–01(**rusting class).

2.6. SEM and EDX analysis of unmodified and modified MF, bpy, Cu(II), and Zr(IV) complexes epoxy coated steel films

Morphological properties of neat untreated (conventional) and surface modified MF, bpy, Cu(II), and Zr(IV) complexes coated films were studied using salt spray severe conditions (aggressive fog of 5% NaCl for 21 days direct exposure) by SEM analysis. Micrographs of the inspected coated steel specimens were illustrated at 800 X magnification. EDX analysis was performed for confirming the modification process in addition to investigating the amount of rust formed on the coated panels.

2.7. AFM analysis for the coating samples after salt spray exposure

Atomic force spectroscopy (AFM) analysis was applied to illustrate 3D- images using Parapola fit for the various coated samples for detecting the surface microstructure and roughness, corroded areas and homogeneity of the coating. The coated steel panels were investigated under a Shimadzu SPM-9600 microscope with 400 nm resolution (minimum limit), outfitted by a 125 μm scanner operating in non-contact mode.

2.8. Acid chemical resistance properties of the coated steel panels

Acid spot resistance test for the employed coated steel panels was proceeded using different types of acids (**ASTM D1308-02e1),** employing the accounting levels as: No determined variation (**Level 0**); few color and gloss variation **Level 1**); Few surface maculation and etching (**Level 2**); Full coating deterioration, swelling, cratering, erosion and pitting **(Level 3)** (ASTM D1308–02e, 2002).

3. Results and discussion

All the separated mixed ligand metal complexes offered air-stability and solubility in DMF and DMSO solvents only. The physical and elemental analysis results of the MF, bpy and their Cu(II) and Zr(IV) complexes were summarized in Table 1. The elemental data emphasize the proposed chemical formula of metal complexes. The stoichiometry of all complexes represented as 1: 1: 1 M^{n+}: MF: bpy as shown in Scheme 1c and d. Molar conductance displayed vital information about chelates arrangement around central metal ions and geometry in addition to indicating the location of anions around the coordination sphere (inside or outside or absent) (Geary, 1971). Conductance estimations of the MF and bpy ligands in DMSO solvent ($1x10^{-3}$ M) were measured at 9.56 and 55.80 S cm^2 mol^{-1}, respectively. Molar conductance of $1x10^{-3}$ M DMSO solution of the complexes was found at 121.12 and 148.80 S cm^2 mol^{-1} consistent with 1:2 electrolytes (Deacon and Phillips, 1980). These data were robustly supported with the test for Cl^- ions by $AgNO_3$ solution (El-Shwiniy et al., 2020). The effective magnetic moment (μ_{eff}) of the Cu(II) complex was measured at room temperature, and found at 1.70 B.M. (paramagnetic), which was consistent with a distorted (elongated) octahedral geometrical arrangement (Magdy Shebl et al., 2016) as illustrated in Table 1. Furthermore, Zr(IV) complex was measured and demonstrated diamagnetic properties with octahedral structure geometry.

3.1. FT-IR spectra

Table 2 illustrated the FT-IR spectra values of MF, bpy and their Cu(II) and Zr(IV) complexes. Comparisons between the spectra of complexes and free MF and bpy ligands were made for detecting the coordination sites involved in chelation process. The intensities and positions of some peaks were changed owing to coordination as shown in Fig. 1. All the stretching bands of imine and amine groups presented in complexes were shifted compared to free MF ligand. The shifting of the $\nu_{as}(NH_2)$, $\nu(NH)$, $\nu_s(NH_2)$ bands of the MF at 3376, 3303, and 3172 cm^{-1} to lower values in the complexes indicated the coordination of MF to the metal (Shahabadi and Heidari, 2014; Vasantha et al., 2018; Olar et al., 2005; Al-Qadsy, 2020; Olar et al., 2010). The shifting of the imine peak (C = NH) of the MF at 1631 and 1573 cm^{-1} to higher values in the complexes indicated that MF is chelated to the metal ions through the nitrogen atom of two imine groups (Vasantha et al., 2018). The FT-IR spectrum of bpy offered peak at 1578 cm^{-1} referred to ν(C = N) groups of pyridine rings, was shifted to 1594, 1580 and 1570 cm^{-1}, respectively, and showed that the bpy was chelated to the metal ion through nitrogen atoms of (C = N) groups as a bidentate ligand (El-Shwiniy et al., 2020; Sadeek et al., 2019; Abd El-Hamid et al., 2019). According to spectra, MF and bpy proceeded

Table 1 Elemental analysis and physico-analytical data for MF, bpy and their metal complexes.

Compounds M.Wt. (MF.)	Color (yield %)	M.P. (°C)	(calcd) % found				Λ S cm^2 mol^{-1}	μ_{eff} (B.M)
			C	H	N	Cl		
MF	white	224	(29.00)	(7.25)	(42.30)	(21.45)	55.80	–
165.50($C_4H_{12}N_5Cl$)			28.90	7.18	42.15	21.35		
Bpy	White	72	(76.89)	(5.16)	(17.93)	–	9.56	–
156($C_{10}H_8N_2$)	-		76.81	5.11	17.91			
Cu(II)	Dark blue	230	(34.18)	(5.49)	(19.94)	(14.44)	121.12	1.70
491.55($C_{14}H_{27}N_7O_4Cl_2Cu$)	93		34.11	5.41	19.90	14.37		
Zr(IV)	Pink	300	(34.91)	(4.36)	(20.36)	(14.75)	148.80	–
481.22($C_{14}H_{21}N_7O_2Cl_2Zr$)	90		34.80	4.30	20.31	14.71		

Table 2 Selected infra-red absorption frequencies (cm^{-1}) of MF, bpy and their metal complexes. Keys: s = strong, w = weak, v = very, m = medium, br = broad, sh = shoulder and ν = stretching.

Compounds	ν(O-H); H_2O;	$\nu_{as}(NH_2)$	ν(NH)	$\nu_s(NH_2)$	ν(C = N); MF	ν(C = N); bpy	ν(M−N), ν(M−O)
MF	–	3376vs	3303 s	3172 s	1631vs 1573 s	–	–
Bpy	3440mbr	–	–	–	–	1578 ms	–
Cu(II)	3755wbr, 3374sbr	3256 s	3207 s	3147 s	1625vs	1509 ms	608 m, 526w
Zr(IV)	–	3300 s	3171 ms	3125 s	1628vs	1577 ms	639 s, 541w

as bidentate ligands through two nitrogen of imine and (C = N) groups as coordination sites, respectively, with the Cu(II) and Zr(IV) ions. The solid complexes spectra displayed some new bands with various intensities characteristic to ν (MN). The ν(MO) and ν(MN) bands were noticed at 608 and 526 for Cu(II), and 639 and 541 for Zr(IV) complex (El-Shwiniy et al., 2020; El-Shwiniy et al., 2020). The proposed structure and chelation mode of metal ions with two ligands to construct the complexes are represented in Scheme 1c and d.

3.2. UV–visible spectra

At room temperature, the UV–Visible absorption bands of the investigated MF and bpy and their complexes were studied to manifest the stereochemistry of metal complexes. Fig. 2 displayed sundry absorption bands, included absorption bands of the ligands; ligand–metal charge transfer and metal ions d-d transition. As depicted in Table 3, the free MF electronic spectrum showed four bands at 360, 373, 290 and 310 nm which may be characterized to n-π* and π- π* transitions, respectively (Refat et al., 2015). In addition, bpy gives two bands at 347 and 284 nm which appointed to n-π* and π-π* transitions within C = N and C = C groups, respectively

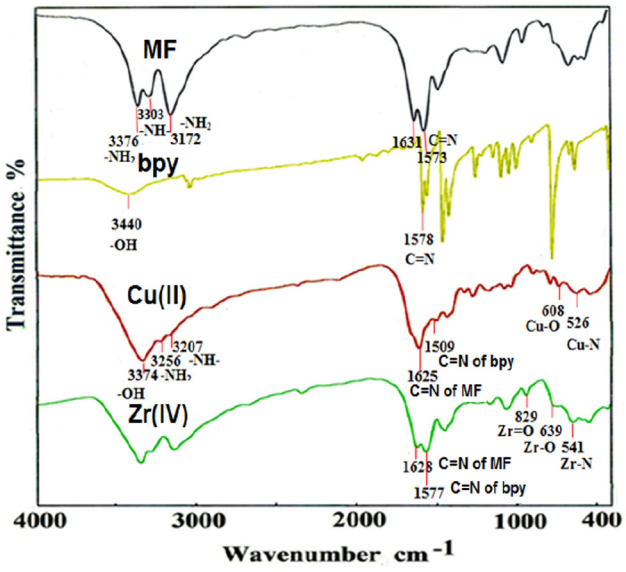

Fig. 1 FT-IR of MF, bpy and their metal complexes.

(El-Shwiniy et al., 2020; Sadeek et al., 2016; Hayashi et al., 2003). Shifting of the bands to lower or higher values and manifestation of new bands for the Zr(IV) and Cu(II) complexes were appointed to the chelation of the ligands (Sadeek et al., 2016; Hayashi et al., 2003). The Cu(II) complex have two bands at 540and 620 nm which appointed to $^2B_{1g} \rightarrow {}^2E_{1g}$ transition and displayed magnetic moment value at 1.70B.M., that characteristic to a distorted (elongated) octahedral geometry (Magdy Shebl et al., 2016; Sadeek et al., 2015; A. Sadeek et al., 2015; Sadeek, 2005).

3.3. ^1H NMR spectra

At room temperature, ^{1}H NMR spectra of MF, bpy and their complexes were recognized in DMSO d_6 as depicted in Table 4 and shown in Fig. 3. MF spectrum showed a signal at 2.93 ppm (s, 6H, $2CH_3$) assigned to methyl protons. Additional resonance arisen from the imines protons at 7.22 ppm (s, 2H, C = NH). The bpy spectrum displayed signals in range of 7.12–8.70 ppm which characterized to the aromatic ring protons (Olar et al., 2010; El-Shwiniy et al., 2020). The ^{1}H NMR spectra of the complexes showed the shift of the broad peak of MF characterized to imine protons from 7.22 ppm to downfield in the spectrum indicated their coordination through imine nitrogen atoms (Magdy Shebl et al., 2016; Olar et al., 2005). The peak of imine proton at 8.35 and 8.69 ppm was appointed to a hydrogen bond with the oxygen atom of the DMSO group bonded to Cu and Zr, respectively (Magdy Shebl et al., 2016). The existence of water molecules in complexes was indicated by the appearance of new bands in the 3.47–3.54 ppm range (Defazio and Cini, 2002).

3.4. TGA/DTG analysis of compounds

The thermal behavior of MF, bPy, and their solid metal complexes was investigated using TGA technique in which the thermo-analytical data described the thermal decomposition steps of these compounds. The TGA/DTG curves of the investigated compounds were displayed in Fig. 4 and depicted in Table 5. The TGA curve of MF indicated that its thermal decomposition achieved through one step. This step occurred at maximum 330 °C with weight loss by 99.24 % (calc 100%) due to removal of $2C_2H_4 + NH_3 + 2\ N_2$ (El-Shwiniy et al., 2020). The TGA/DTG analysis of bpy was discussed in the literature (Sadeek et al., 2019; Abd El-Hamid et al., 2019), which presented one degradation stage at

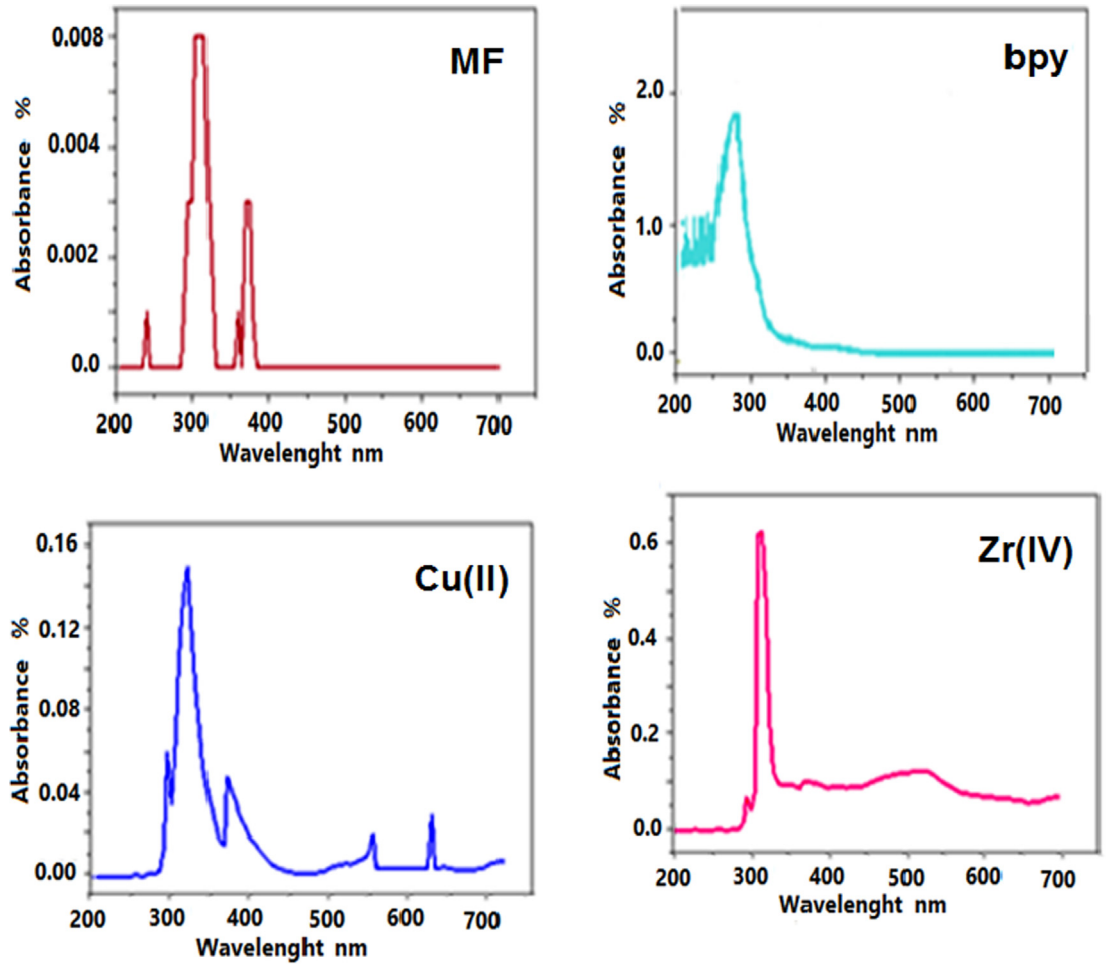

Fig. 2 Electronic absorption spectra for MF, bpy and their metal complexes.

164 °C with weight loss of 99.64% (calc 100%), and calculated activation energy (E^*) at 75.70 KJ mol^{-1}. The thermal behaveir of the complexes could be sub-divided into three stages. The first step accompained by the mass loss of hydrated H_2O molecules and the second decomposition step took place with lost species $2C_2H_2$ + HCl + $2NH_3$ + 1.5 N_2 and $3C_2H_4$ + 2.5 N_2 for Cu(II) and Zr(IV), respectively. In addition, the third step indicated by TGA was corresponding to the degradation of $2C_2H_4$ + HCl + NH_3 + NO_2 and HCl + NH_3 + $0.5H_2$ with leaving Cu + 6C, and ZrO_2 + 3C respectivly, as a final product. To determine the effect of the complexes structural properties on the thermal demeanor in which the activation energy E^*, entropy ΔS^*, enthalpy ΔH^*, and Gibbs free energy ΔG^* of the decomposition stages were determined from the TGA and DTG thermo-grams using Coats–Redfern and Horowitz–Metzger equations (COATS and REDFERN, 1964; Horowitz and Metzger, 1963). Table 6, illustrated the thermodynamic parameters of the decomposition stages for Cu(II) and Zr(IV). The decomposition entropies showed -ve values that indicated the reactions were slower than normal (Moore and Pearson, 1981). The activation energies of decomposition of the complexes were found in the range 68.75–98.5 KJ mol^{-1} (CR). The elevated E^* values for the investigated complexes gave an indication about the thermal stability of these complexes (Omar, 2009; Rotaru et al., 2008). The positive values of ΔH^* reflected that the

Table 3 UV–Vis. spectra of MF, bpy and their metal complexes.

Assignments (nm)	MF	bpy	Cu(II)	Zr(IV)
π-π* transitions	290	284	295	295
n-π* transitions	310, 360, 373	347	320, 370	320, 370
Ligand-metal charge transfer	–	–	540	523
d-d transition	–	–	620	–

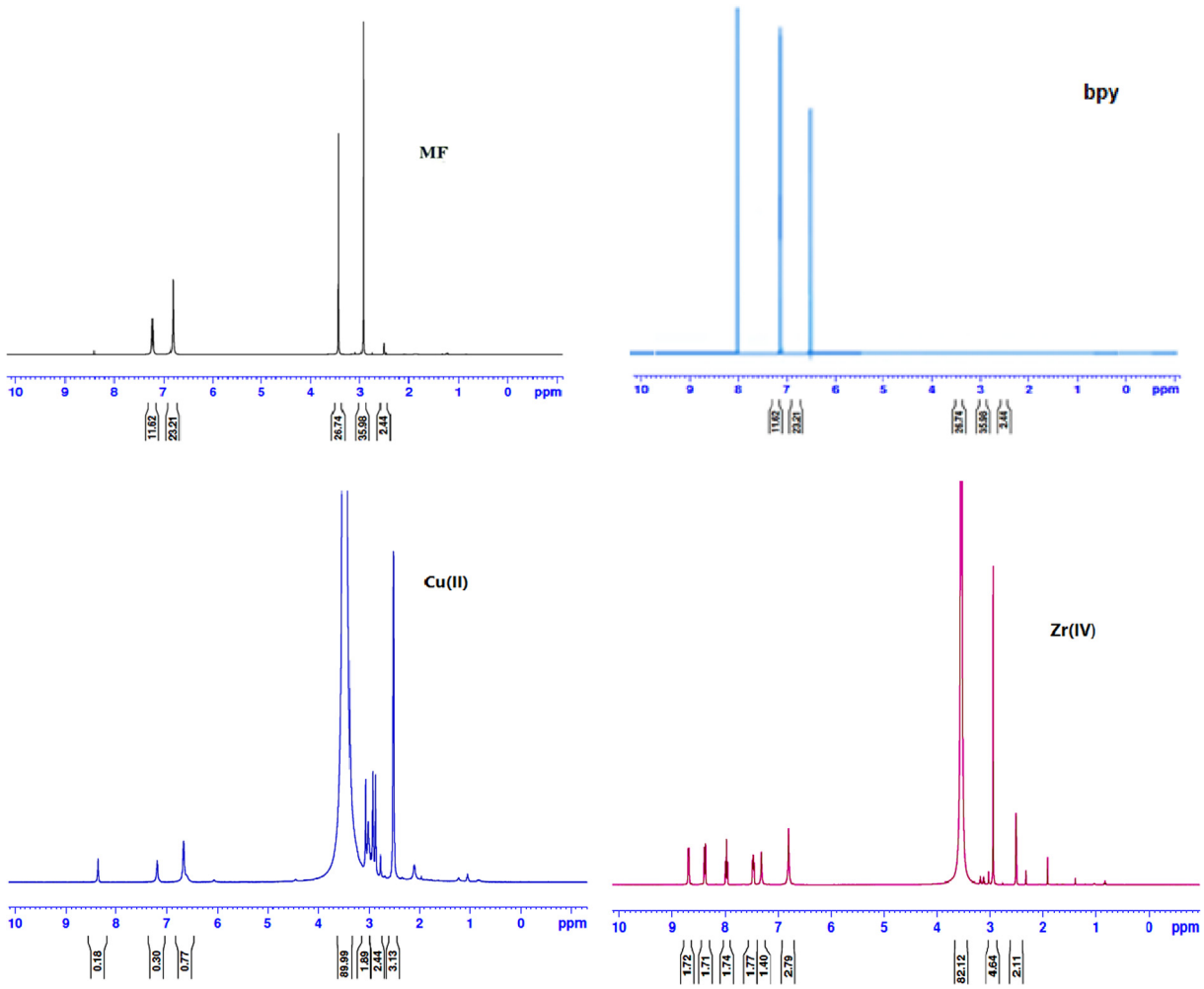

Fig. 3 ^{1}H NMR spectra for MF, bpy and their metal complexes.

decomposition processes of the investigated ligands and their complexes were endothermic (A. Sadeek et al., 2015; Mahmoud et al., 2014).

3.5. Structural parameters and models

3.5.1. Structure geometry of MF and bPy

The parameters of structure geometry and the optimized geometry of MF and bpy ligands using DFT calculations were listed in Table 7 and illustrated in Fig. 5. Torsion angles varied between $-0.004° \approx 0.00°$ and $179.99° \approx 180.00°$ in case of MF and varied between 0.00° and 180.00° in case of bpy affirmed the planarity of the two free ligand molecules (Abd El-Hamid et al., 2019). Variation in bond angles between 117.95° and 123.47° affirmed the sp^2 hybridization sort of atoms. All atoms in MF were not arranged in chain shape but the variation in angles between atoms was recognized between 114.00° and 137.53° and reflected that most atoms had sp^2 hybridization sort. The MF five donating centers were provided from the theoretical investigation. It was observed that the MF could proceed as bi-dentate ligand via the two adjacent nitrogen atoms (N5, N9) of C = NH groups, which were lying in the same direction. Also, bpy had two donating nitrogen atoms (N1 and N4) (Abd El-Hamid et al., 2019). According to the observed results, there was a good agreement between the experimental and computed geometrical

Table 4 ^{1}H NMR values (ppm) and tentative assignments for MF, bpy and their metal complexes.

MF	bpy	Cu(II)	Zr(IV)	Assignments
2.93	–	2.92	2.93	δH, –CH_3 methyl
–	–	3.47	3.54	δH, H_2O
–	7.12–8.70	6.65, 7.18	6.80–7.48	δH, –CH aromatic
7.22	–	8.35	8.69	δH, =NH imine

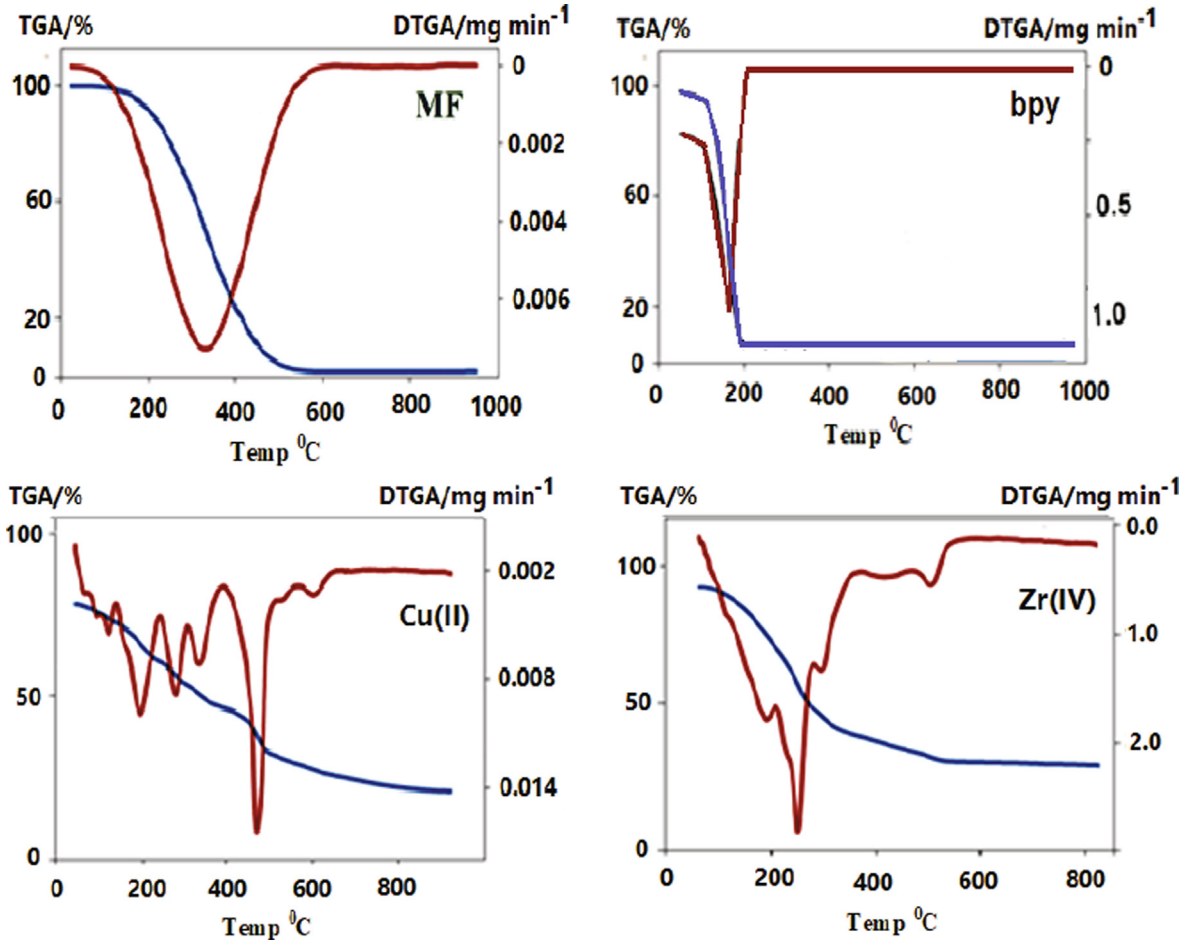

Fig. 4 TGA and DTG analysis for MF, bpy and their metal complexes.

parameters. The mean average deviation between the B3LYP/CEP-31G and experimental bond lengths and bond angles were 0.06 Å and 0.3°, and these results were portrayed to illustrate the optimized geometry of molecules.

The optimized geometry of MF and bpy and charge distributions localized on the donating nitrogen atoms were calculated. There was a considerable installation of charge density on N5 and N9 of MF ligand, −0.528 and −0.519, respectively and on N1 and N4 of bpy, −0.210 and −0.212, respectively. These charge density values reinforced the chelation between MF and metal ion via the two nitrogen atoms of the two C = N groups as bi-dentate and chelation of bpy through two nitrogen atoms of the two pyridine rings.

Table 5 The maximum temperature T_{max} (°C) and weight loss values of the decomposition stages for MF, bpy and their metal complexes.

Compounds (M.F)	Decomposition	T_{max}(°c)	Weight loss (%)			Lost species
			Calc.	Found	Total loss	
MF	First step	330	100	(99.24)	100 (99.24)	$2C_2H_4 + NH_3 + 2\ N_2$
Bpy	First step	164	100	99.64	100 (99.64)	$4C_2H_2 + C_2N_2$
Cu(II)	First step	100	7.32	7.40		$2H_2O$
	Second step	159, 218, 261	33.47	33.42		$2C_2H_2 + HCl + 2NH_3 + 1.5\ N_2$
	Third step	361, 460	31.63	32.25	72.42 (73.07)	$2C_2H_4 + HCl + NH_3 + NO_2$
	residue		27.58	26.93		Cu + 6C
Zr(IV)	First step	195	23.59	23.90		$2C_2H_2 + NCCl$
	Second step	265, 319	32	32.47		$3C_2H_4 + 2.5\ N_2$
	Third step	463, 568	11.33	10.55	66.92 (66.92)	$HCl + NH_3 + 0.5H_2$
	Residue		33.09	33.08		$ZrO_2 + 3C$

Table 6 Calculated thermal behavior and Kinetic parameters for MF, bpy and their metal complexes using Coats–Redfern (CR) and Horowitz–Metzger (HM) equations.

Compounds	Decomposition Range (K)	T_s (K)	method	Parameters					R^a	SD^b
				E* (KJ/mol)	A (s^{-1})	ΔS* (KJ/mol. K)	ΔH* (KJ/mol)	ΔG* (KJ/mol)		
MF	350–980	603	CR	25.59	0.118	−0.263	22.85	109.84	0.993	0.10
			HM	30.63	3.98×10^2	−0.196	27.89	92.56	0.984	0.20
Bpy	315–554	437	CR	75.70	6.53×10^6	−0.118	72.06	123.46	0.998	0.094
			HM	95.74	2.79×10^9	−0.067	92.11	121.49	0.998	0.106
Cu(II)	581–704	634	CR	99.55	2.71×10^5	−0.142	96.55	147.980	0.927	0.354
			HM	80.10	4.79×10^9	−0.061	77.10	99.18	0.923	0.396
Zr(IV)	490–578	538	CR	68.95	1.1×10^4	−0.166	66.74	110.90	0.944	0.277
			HM	43.71	5.1×10^6	−0.115	41.51	72.10	0.995	0.307

a = correlation coefficients of the Arrhenius plots and b = standard deviation.

3.5.2. Complexes geometry

Explication of the equilibrium geometry and discussion of charge distribution of each studied compounds represented the main purposes of this investigation. For Cu(II) complex, the Cu ion reacted with one molecule from each MF and bpy forming an elongated octahedral structure. The bond lengths and bond angles (Deghadi et al., 2020; Yan et al., 2016; Khandar et al., 2019) of the investigated complexes were given in Table 8. In Cu(II) complexes, the equatorial plane was conquered by two nitrogen atoms (N1, N4) of bpy molecule, nitrogen atom (N9) of MF molecule and oxygen atom (O10) of water molecule. Also, the axial plane was occupied by nitrogen atom (N5) of MF and (O11) of second water molecule. While ZrO bond linked to one H_2O molecule to complete the distorted octahedral structure. The equatorial plane of Zr (IV) complex occupied by two nitrogen atoms (N1 and N4) of bpy , nitrogen atom (N9) of the MF ligand molecule and oxygen atom (O10) of Zr = O group, the water molecule was trans respect to nitrogen atom N5 of MF ligand.

3.5.3. Charge distribution analysis (CDA)

The CDA over the optimized geometry array of all investigated compounds was made on the basis of natural population analysis (NPA) and reported in Table 9. The CD on MF and bpy indicated the absence of a net negative pole and this could be assigned to the absence of polar atoms beside the high degree of planarity of these molecules and this affirmed that the molecules were weakly dipole (μ = 5.900 D for the MF). The given charge densities for the ligands and their complexes illustrated in Table 9 showed a significant building up of charge density on the all nitrogen atoms of the MF and bpy. There was a relatively high charge density on the Zr(IV) complex at 0.301. The lower charge density and the smallest value was located on Cu(II) complex (0.021). Also, the negative charges on surrounding nitrogen atoms of MF in all studied complexes were greater than that on nitrogen atoms of bpy. This result contemplated that there was a sturdy interaction between central metal ions and nitrogen atoms of the MF more than that of bpy. The negative charge was localized on

Table 7 Equilibrium geometric parameters bond lengths (Å), bond angles (), dihedral angles (), total energy (au), heat of formation (k cal/mol) and dipole moment of the MF by using DFT calculations.

Bond length (Å)			
C1-N9	1.288	C6-N7	1.358
C1-N3	1.338	C8-N7	1.471
N4-C6	1.346	C2-N7	1.448
C6-N5	1.292		
Bond angle ()			
N3C1N9	114.00	N4C6N7	134.77
N9C1N4	114.63	C6N7C8	118.48
C1N4C6	137.53	C6N7C2	121.64
N4C6N5	108.07	C2N7C8	119.89
Dihedral angles ()			
C3C1N4C6	−0.007	C1N4C6N7	0.010
N9C1N4C6	179.99	N4C6N7C8	179.99
C1N4C6N5	−179.99	C2N7C6N4	−0.004
Total energy/ eu		−86.819	
Heat of formation k cal/mol		−3142.411	
Total dipole moment/D		5.900	

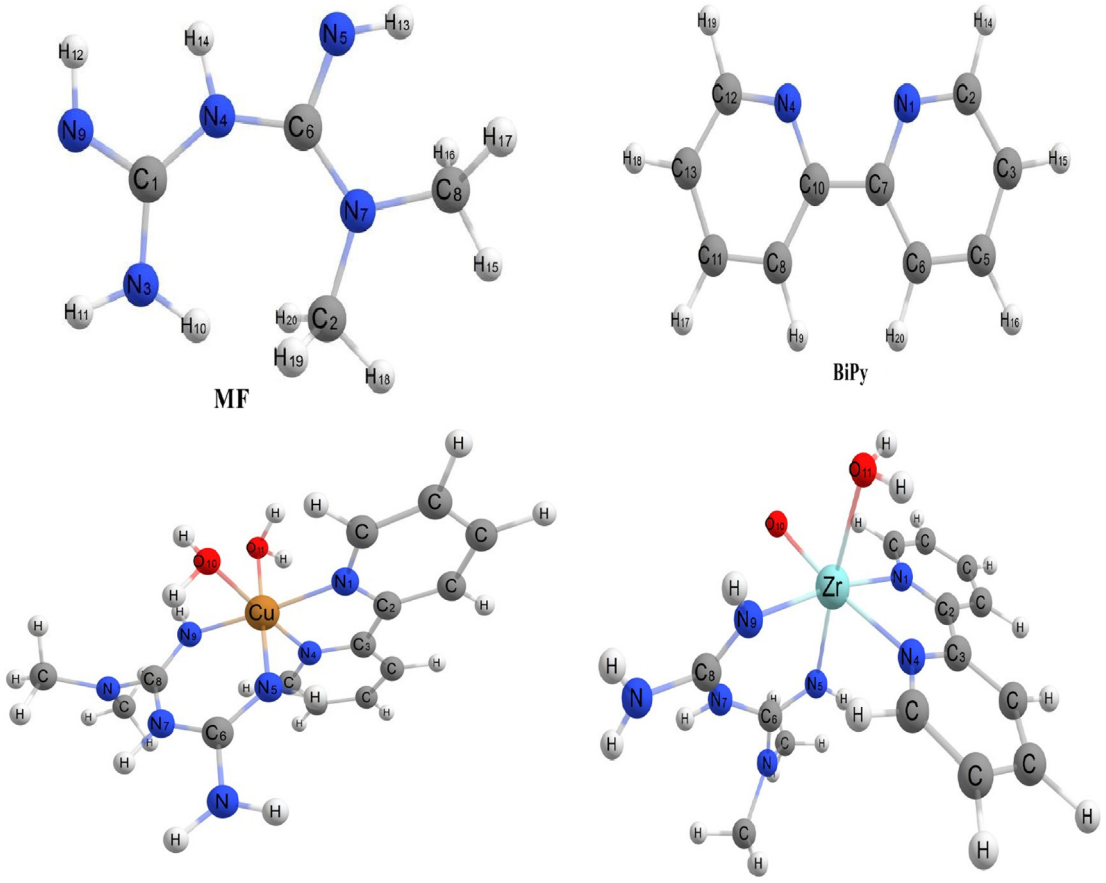

Fig. 5 DFT-optimized geometry of MF, bpy and their metal complexes.

nitrogen atoms of the two ligands, while all the carbon and hydrogen atoms in all complexes hold + ve charge. For the investigated complexes the nitrogen atoms (N5 and N9) of MF had more -ve charge than nitrogen atoms (N1 and N4) of bpy and the carbons directly attached to nitrogen atoms in the two ligands had more + ve values owing to the electronegative character of nitrogen atoms. The data indicated that there was an electron back-donation from the metal sites in a MLCT mode to the π* orbitals of the MF in some of these complexes. This deduction was further assured by comparing the values of the measured charge density on the donating nitrogen atoms of this ligand. Also, the atomic charges distribution was remarkable to determine the dipole moment vector direction in the complexes which depended on the centers of negative and positive charges.

3.5.4. Molecular orbitals (MOs) and frontier

MOs play a vital role for investigating the electronic properties as illustrated in UV–Vis analysis (Fleming, 1976). Accordingly for the electronic system, the greater values of HOMO-LUMO (ΔE) gap made the system to be less reactive than that with lower ΔE values (Kurtaran et al., 2007). The measurements of the stability and reactivity of complex molecules relied on the calculated value of ΔE in addition to offering the molecule nature with little chemical reactivity and depressed kinetic stability. Also, the adjacent orbitals were oftentimes closely splayed on the frontier region. The variation in ΔE estimations for the complexes depended on metal ion type as depicted in Table 9. The checked complexes had lower ΔE less than free ligands, so the reactivity of these complexes was higher than that of free ligands. The energy gaps (ΔE) of the Cu(II) and Zr(IV) complexes were measured at 0.190 au which indicated that these complexes were more reactive. So, diminishing the ΔE value facilitated the electron movement between these orbitals. The ΔE of MF and bpy were calculated at 0.365 and 0.280 au, respectively and this displayed that these ligands were less reactive.

The nodal properties of molecular orbitals of complexes as shown in Fig. 6 were illustrative and suggested orbital delocalization, strong orbital overlap, and low number of nodal planes. Fig. 6 showed the *iso*-density surface plots of HOMO and LUMO for the free ligands and their Cu(II) and Zr(IV) complexes. For the MF, the electron density of HOMO was delocalized and spread over the all fragments of MF except middle –NH- group, and also, in case of the electron density of LUMO for MF, there was a delocalization of electron density and spreading over all atoms except middle –NH- group. Hard molecules had high ΔE gap, and soft molecules had smaller ΔE gap (M. Abd El-Hamid et al., 2020). The values of η and ΔE given in Table 9 indicated that Cu(II) and Zr (IV) complexes were soft in which ΔE was calculated at 0.190 and η measured at 0.095 au, while η for free MF and bpy were η = 0.183 and 0.140, respectively. There were some quantum chemical parameters such as global softness (S), electronegativity (χ), chemical potential (Pi), absolute softness (σ), global electrophilicity (ω) and additional electronic charge

Table 8 Equilibrium geometric parameters bond lengths (Å), bond angles (),dihedral angles (), Total energy (eV) , Heat of formation (k cal/mol) and Dipole moment of the studied complexes by using DFT calculations.

Bond lengths/ Å	Cu(II)	Zr(IV)
M−N1	2.293	2.315
M−N4	2.289	2.319
M−N5	1.951	2.331
M−N9	1.948	2.335
M−O10	2.253	2.121
M−O11	2.250	2.095
C2-N1	1.287	1.287
C3-N4	1.286	1.285
C6-N5	1.344	1.344
C8-N9	1.347	1.345
Bond angles ()		
N1-M−N4	78.47	71.01
N1-M−N5	89.31	87.89
N1-M−N9	173.47	171.59
N1-M−O10	98.51	102.12
N1-M−O11	88.18	90.91
N4-M−N5	90.72	85.99
N4-M−N9	99.69	101.73
N4-M−O10	177.26	172.75
N4-M−O11	92.36	87.95
N5-M−N9	97.07	87.13
N5-M−O10	89.29	97.23
N5-M−O11	175.58	172.85
N9-M−O10	83.03	85.31
N9-M−O11	85.54	93.19
O10-M−O11	87.48	89.91
Total energy, eV	−277.638	−225.691
HF, k cal/mol	−8089.334	−7465.958
Dipole moment, D	4.249	10.058

(ΔN_{max}) of the free ligands and complexes depending on the calculated HOMO and LUMO energy values.

3.6. Formulation basis for PA-DGEBA/MF, PA-DGEBA/bpy, PA-DGEBA/MC-Cu, and PA-DGEBA/MC-Zr coatings

The epoxy vehicle carried the investigated coating ingredients was of diglycidyl ether of bisphenol-A (DGEBA), in which represented the most applied type of epoxies and always required specific modification for resisting the harsh conditions (aggressive species, chemicals and mechanical efforts). The discussed MF and bpy ligands and their mixed Cu(II), and Zr(IV) complexes were dissolved in solvent mixture composed of 20 isobutanol: 30 THF: 50 DMSO to be compatible with epoxy resin for obtaining the surface-modified homogeneous epoxy coating formulations. The employed checked ligands and their mixed complexes offered novel modified performance for epoxy coating in which acted as muting agents and super cross-linking agents (accelerators) to consolidate the density of cross-linking of the polyamine/epoxy adduct. They also improved the coating film stiffness. Xylene solvent was used for viscosity controlling. The coating polarity enhancement was achieved by using isobutanol and the solvation power was attained using tetrahydrofuran (THF) solvent. Improvement in the coating surface properties and induction period could be fulfilled using ethylene glycol (Fadl et al., 2020). Di-isononyl phthalate (DINP) plasticizer was anticipated as coating layer flexibility promoter. Ancamine 1734 hardener was employed for complete curing process and building up a boosted three-dimensional network with DGEBA. The expected cross-linking routes by using MF, bpy ligands and their mixed complexes were illustrated in Scheme 2. The terminals of amino-groups of polyamine curing agent and the other

Table 9 Calculated charges on donating sites and energy values (HOMO, LUMO, Energy gap ΔE/au, hardness (η), global softness (S), electronegativity (χ), absolute softness (σ), chemical potential (Pi), global electrophilicity (ω) and additional electronic charge (ΔN_{max}) of the two ligands and studied complexes by using DFT calculations.

Parameters	MF	Bpy	Cu(II)	Zr(IV)
M	-	-	0.021	0.301
N1	-	−0.210	−0.107	−0.105
N4	-	−0.212	−0.071	−0.088
N5	−0.528	-	−0.376	−0.324
N9	−0.519	-	−0.358	−0.318
O10	-	-	−0.325	−0.412
O11	-	-	−0.328	−0.260
HOMO, H	−0.382	−0.425	−0.359	−0.387
LUMO, L	−0.017	−0.145	−0.169	−0.197
I = -H	0.382	0.425	0.359	0.387
A = -L	0.017	0.145	0.199	0.197
ΔE = L-H	0.365	0.280	0.190	0.190
η = (I-A)/2	0.183	0.140	0.095	0.095
χ = -(H-L/2)	0.199	0.285	0.294	0.292
σ = 1/ η	5.465	7.143	10.526	10.526
S = 1/2 η	2.732	3.571	5.263	5.263
Pi = - χ	−0.199	−0.285	−0.264	−0.292
ω = $(Pi)^2$/2 η	0.108	0.290	0.367	0.449
ΔN_{max} = χ/ η	1.087	2.036	2.779	3.074

(I) is ionization energy, (A) is an electron affinity.

of the employed ligands and their complexes formed polyamine cured epoxy composite distinguished as hard sealant epoxy layer as shown in the molecular structures and 3D models offered in Scheme 3.

3.7. The corrosion-mitigation behavior

The corrosion mitigation performance of the investigated PA-DGEBA/MF, PA-DGEBA/bpy, PA-DGEBA/MC-Cu and PA-DGEBA/MC-Zr coated films against the blank neat epoxy was discussed to offer the corrosion guard effect of MF, bpy and their mixed Cu(II) and Zr(IV) complexes as additive modifiers incorporated with the same loading level (%) by weight from the coating formulation ratios. The influence of incorporating these species depended on the highly cross-linking density displayed via the synergistic effect by extra-crosslinking of amine terminals of the ligands and their mixed complexes in addition to the original cross-linking by polyamine curing agent to offer hard nonporous protective coating layer. The salt spray accelerated corrosion results after the directly exposure to salt spray aggressive fog (5% NaCl solution and humidity of 95 at 35 °C) for 500 h were illustrated in Table 10 and shown in Fig. 7. Visual inspection was made using the standard reference photographs to evaluate the adhesion grade, the blistering frequency and size, rust class and softening. The blistering frequency is also divided to Dense, Medium, Medium dense and Few. Classification of rust grade including (10 means no rusting < 0.01% of rusted surface; and grade of rust at 0 indicates = 100% of rusted surface. The size of blistering is assorted from #8 to #3, (#8 means no blistering and #3 rates the greatest size of blistering (Wahba et al., 2017). The observed results affirmed that neat epoxy displayed drastic chemical changes (failure), in which the film demonstrated blistring with #3 size and dense frequency, observed softening, grade of rusting (3), and class of adhesion (2B). In addition, intensive corrosion products (brownish $Fe(OH)_3$) and pitting corrosion appeared over the coating layer especially, in the X-cut area due to the penetration of corrosive species and chlorides via tortuous pathways in case of neat epoxy film (Abdou et al., 2017). PA-DGEBA/MF coated film (coating modified with MF ligand) displayed visually the presence of rust with grade (5), layer softening, blisters size of #3 size and medium dense frequency in addition to adhesion class (3B). The dispersion of MF ligand cross-linked with epoxy resin enhanced the corrosion inhibiting demeanor behavior of the coating layer and diminished the deterioration effect by the aggressive fog. PA-DGEBA/bpy coating (coating modified with bpy ligand) offered reinforced protection properties than in case of PA-DGEBA/MF coating in which achieved rust with grade (6), film softening, blister size of #3 size and frequency (medium), and adhesion class (3B). Furthermore, PA-DGEBA/MC-Zr coated layer (coating modified with Zr

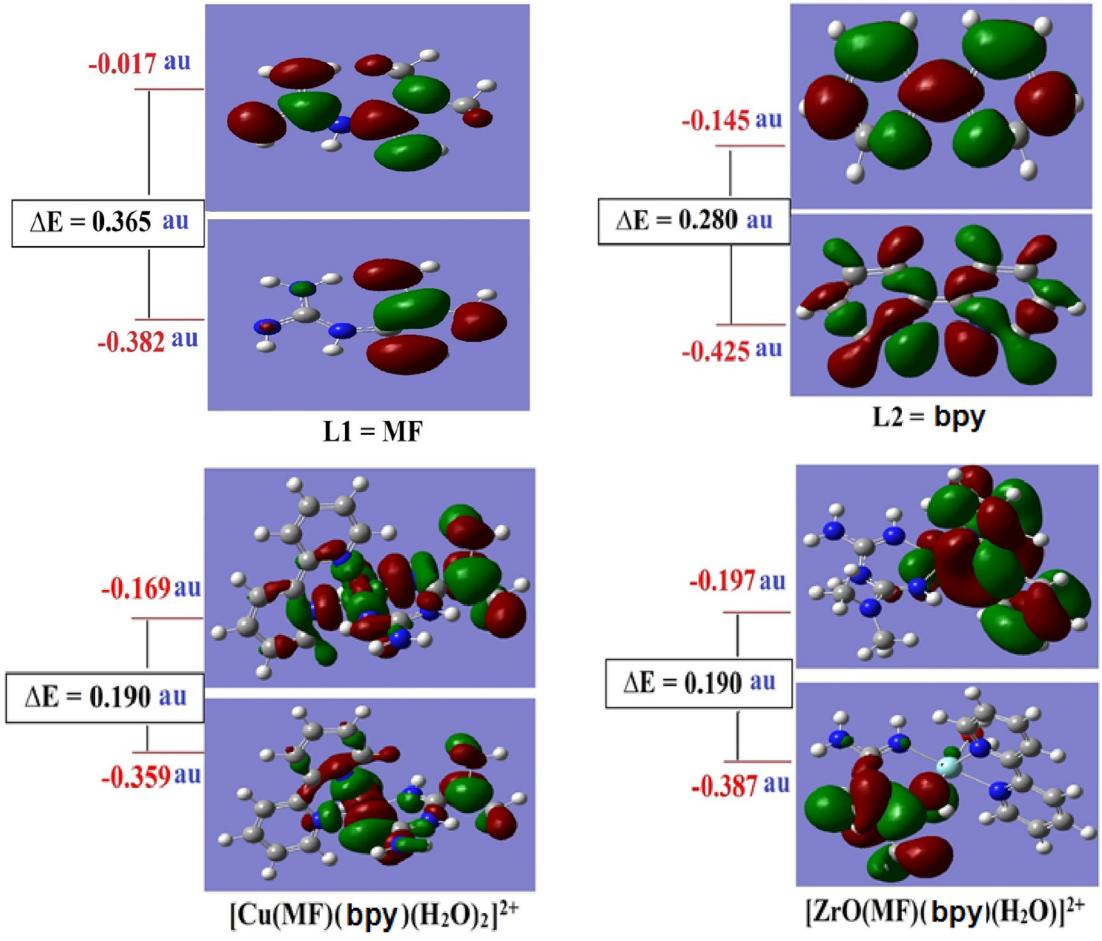

Fig. 6 Molecular orbital surfaces (MOS) and energy levels of MF, bpy and their metal complexes.

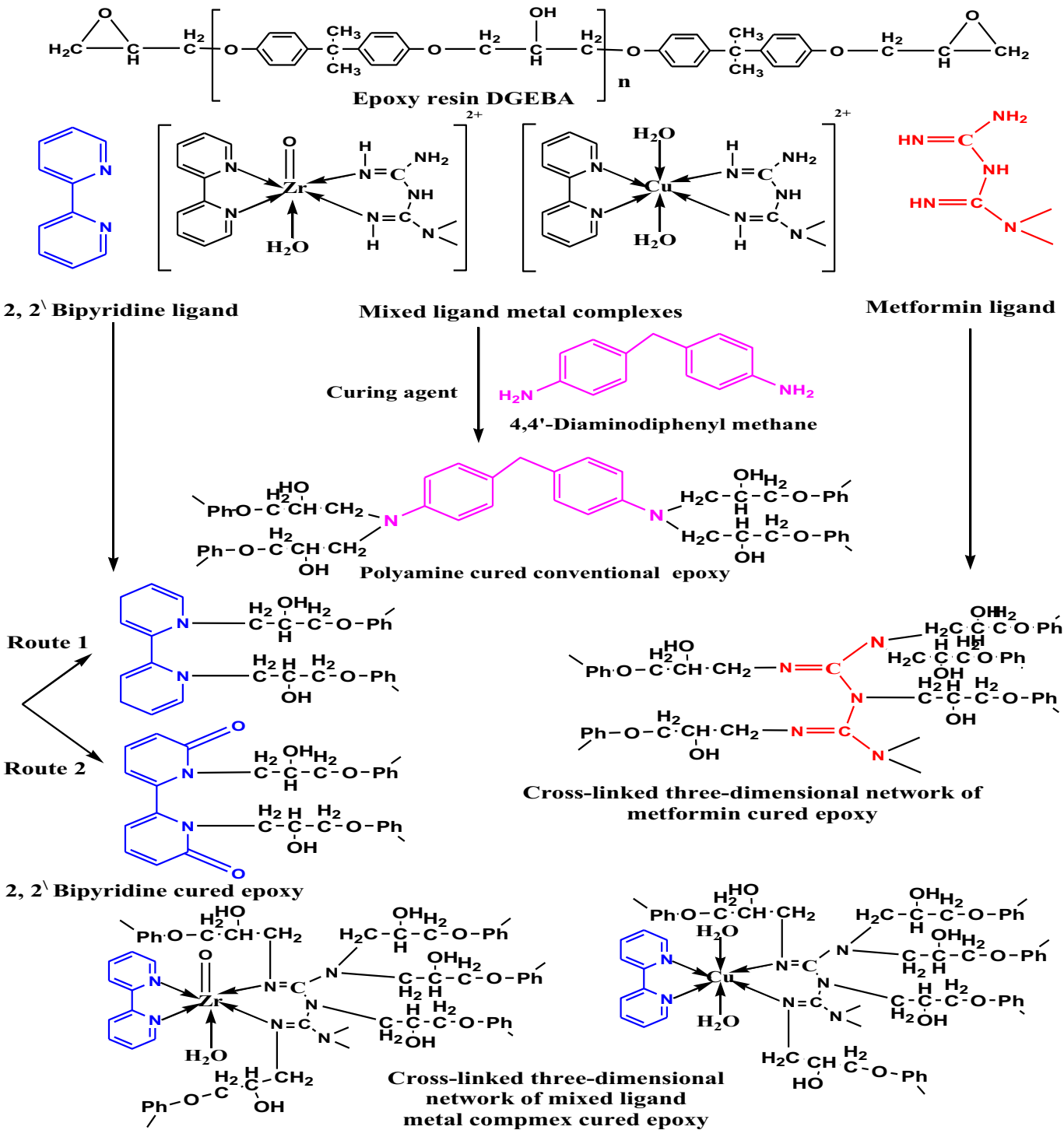

Scheme 2 The suggested three-dimensional networks of cured epoxy with MF, bpy ligands and their mixed Zr(IV), and Cu(II) complexes.

(IV) complex) illustrated visually no softening through the cured coating film and the size of blisters was offered at #4 with few frequency, class of adhesion (5B), and grade of rusting (8). The data depicted in Table 10 demonstrated a superior anti-corrosion behavior for PA-DGEBA/MC-Cu coated film (coating modified with Cu(II) complex) in which achieved rust with grade of 10, no film softening (hard cured film), blister size of #8 size and frequency (few), and adhesion class (5B). As shown in Fig. 7, PA-DGEBA/MC-Cu displayed a self-healing effect via the uncoated scratched area in addition to its pre-emptive behavior on the carbon steel substrate.

SEM micrographs shown in Fig. 8, illustrated qualitative analysis about the effect of modifying the epoxy coating with MF, bpy and their complexes and asserted the corrosion guard demeanor of modified coatings against full spoilage in case of neat epoxy after the directly innuendo to the salt spray severe

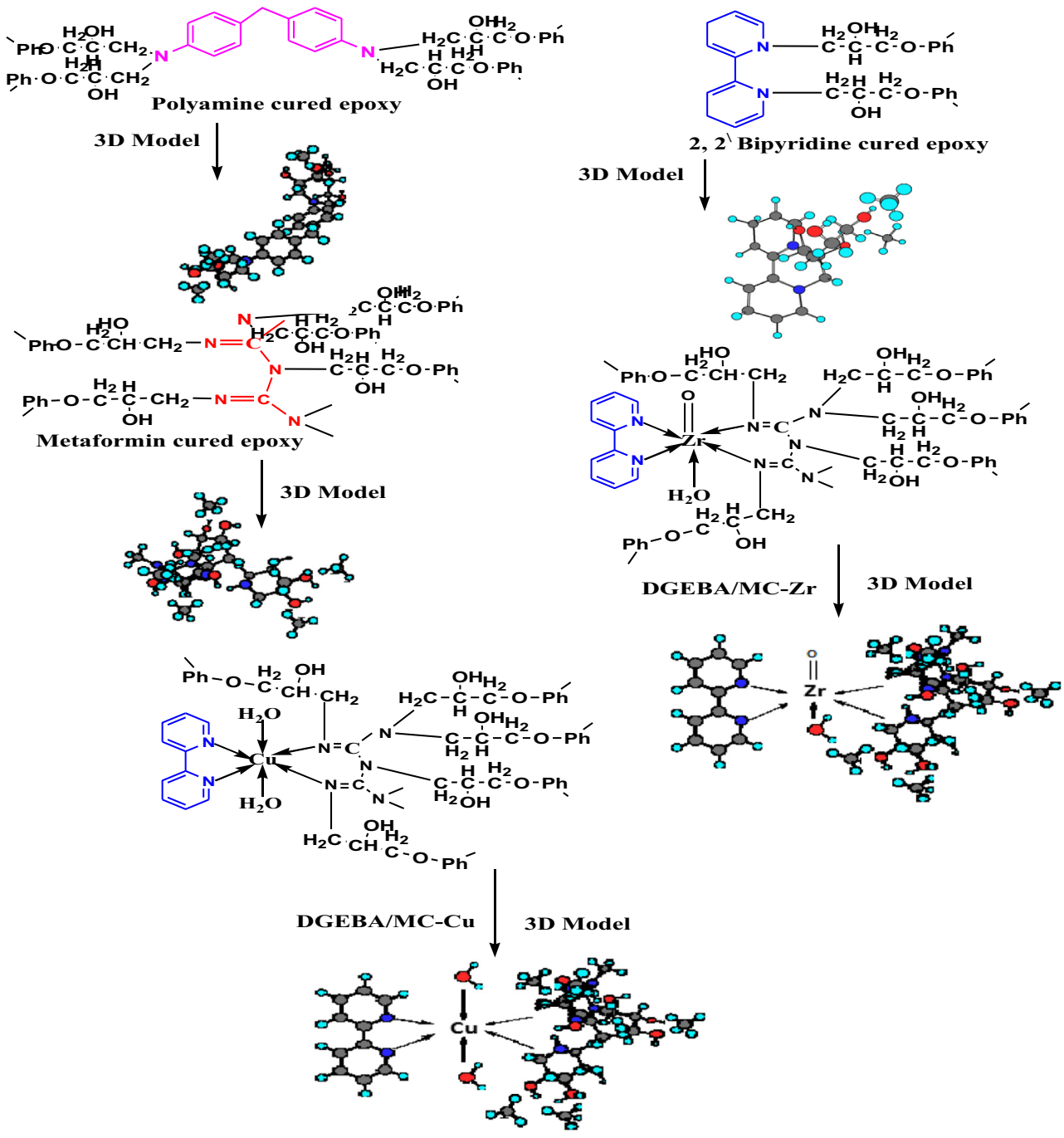

Scheme 3 Molecular structures and 3D models of the polyamine cured epoxy, MF, bpy and their Zr(IV), and Cu(II) mixed complexes.

fog. Blank conventional epoxy offered big cracks with excessive corrosion products observed over the coating surface as shown in Fig. 8a. In this case, the aggressive species permeated the coating and hooked up to the base metal surface and cause full damage owing to corrosion. PA-DGEBA/MF coating manifested the spreading of dense rusting and some few cracks but less than illustrated by the conventional unmodified epoxy as displayed in Fig. 8b. PA-DGEBA/bpy displayed some micro-cracks spread over the top coat with dispersal of upper surface pores and the effect of aggressive fog was lower than in case of PA-DGEBA/MF and blank epoxy coating as displayed in Fig. 8c. The full coating delamination performance in case of PA-DGEBA/MF and blank epoxy coated films and the lower effect observed for PA-DGEBA/bpy coating were because of the increase in pH value under the coating surface producing from the formed NaOH ions generated beneath the coating by the electrochemical reactions (release of OH– anions from undercoat diffused water and Na^+ ions of salt spray fog) (Fadl et al., 2020). Also, the transmission of the corrosive species via the zigzag channels and micropores of these coating layers was occurred, thereby enhancing the ingress of corrosive products and blisters under coating

Table 10 Accelerated corrosion test of unmodified and surface modified MF and bpy and their mixed metal complexes epoxy coated films after 500 h direct exposure in salt spray cabinet using 5% NaCl solution.

Coating code	Blistering		Rust grades	Softening	Adhesion cross-cut
	Size	Frequency			
Blank epoxy coating	#3	Dense	3	Observed	2B
PA-DGEBA/MF	#3	Medium Dense	5	Observed	3B
PA-DGEBA/bpy	#3	Medium	6	Observed	3B
PA-DGEBA/MC-Zr	#4	Few	8	Observed	5B
PA-DGEBA/MC-Cu	#8	Few	10	Not observed	5B

and progressing of micro-cracks. As shown in Fig. 8d, PA-DGEBA/MC-Zr coating exhibited an enhancement in the protective behavior in which there was some micro-pores diffusing over the coating surface without presence of micro-cracks. The ultra-protective behavior of PA-DGEBA/MC-Cu coating was illustrated in Fig. 8e, in which perfect protected coating layer was observed without spreading of any micro-voids or micro-cracks. The checked morphological images affirmed the formation of an integral organic (DGEBA)–inorganic (metal complex) intercross-linked networks and supported the corrosion guard behavior (Ramezanzadeh et al., 2019). In addition, the complex filling diminished the epoxy loading

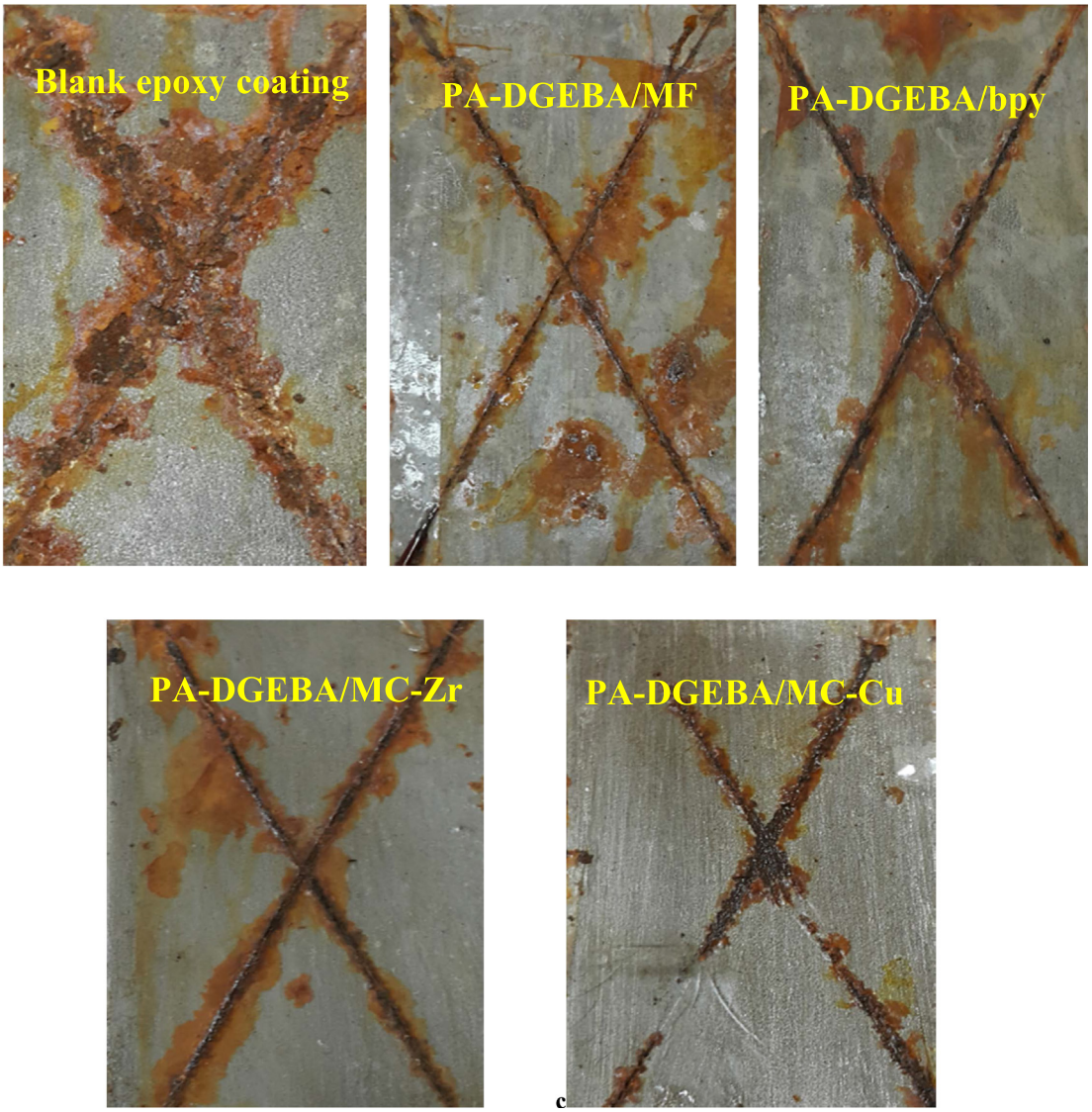

Fig. 7 Salt spray accelerated corrosion experiment for the investigated surface modified epoxy coated panels against blank unmodified coating after direct exposure to aggressive fog (5% NaCl solution and humidity of 95 at 35 ^{O}C).

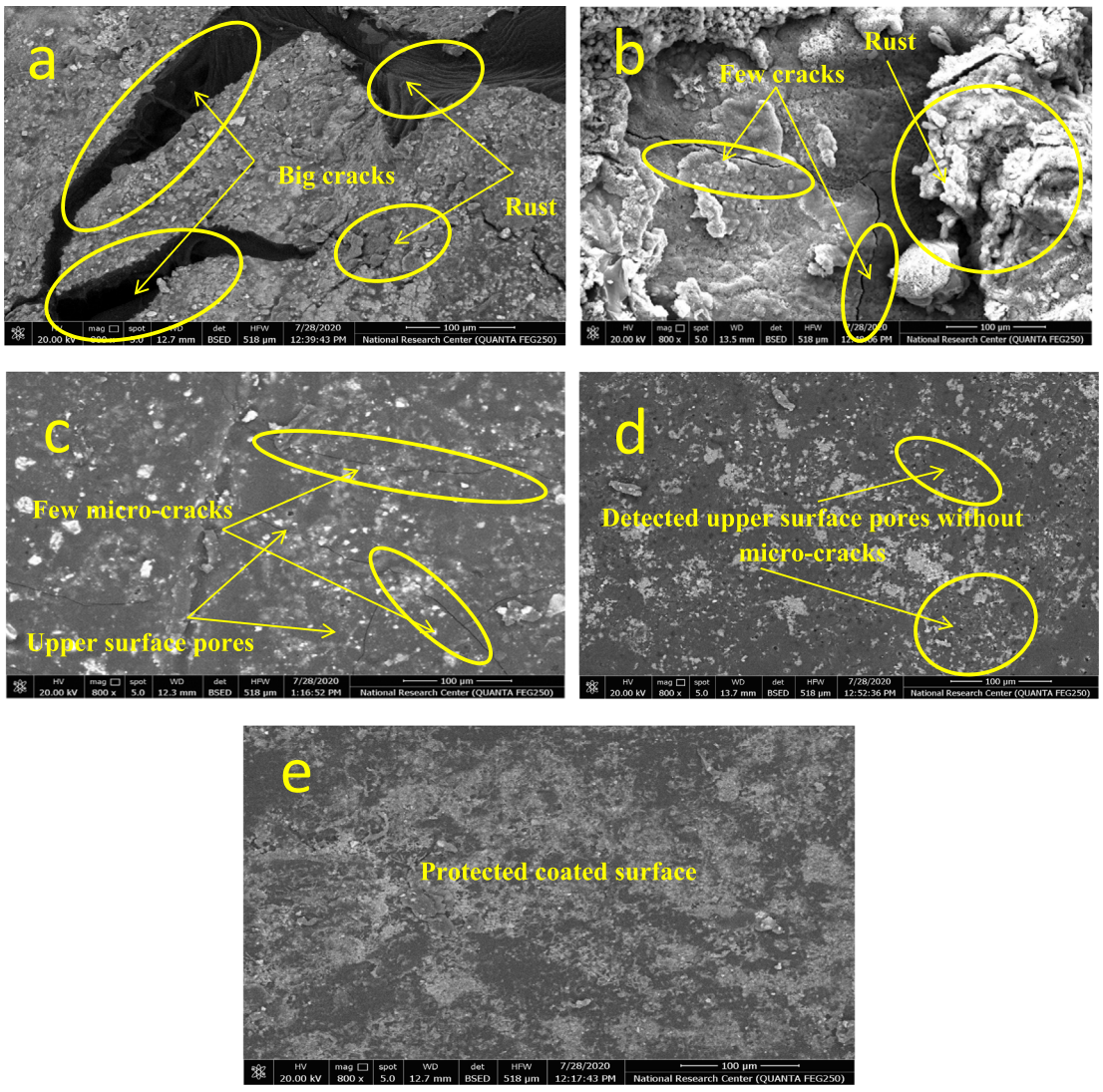

Fig. 8 SEM images of the investigated coated films a) Unmodified conventional epoxy, b) PA-DGEBA/MF, c) PA-DGEBA/bpy, d) PA-DGEBA/MC-Zr and e) PA-DGEBA/MC-Cu after the direct exposure to salt spray fog at severe conditions.

stress by corrosive fog species produced from cabinet nozzles (Depoorter et al., 2006).

EDX quantitative analysis was carried out to measure the corrosion mitigation behavior with incorporating of MF, bpy and their mixed complexes through the coating film (Abdou and Fadl, 2019) as shown in Fig. 9. The Fe peak intensity (detected by arrow) displayed the protective performance of the coating layer with the same thickness and also with the same loading level (%) by wt. of the investigated modifier species (high peak count offered low inhibition and vice versa). Furthermore, EDX elemental survey displayed the chemical analysis of the epoxy coating film on the C-steel substrate to clarify the modification process of coating with ligands and their mixed metal complex molecules and other presented elements due to the directly innuendo to corrosive fog against non-modification of neat epoxy. In addition, EDX survey gave quantitative indication about the inhibition efficiency of the coating film over the steel substrate. The EDX analysis of conventional epoxy coating displayed the highest iron count at 23.8 which confirmed the least protective performance as displayed in Fig. 9a. The elemental analysis of unmodified conventional coating demonstrated the appearance of high percentages (as peaks) of Na and Cl^- ions (represented to the aggressive sodium chloride solution of salt spray cabinet). In addition, iron oxide moieties (source of rusting as $Fe(OH)_3$ in presence of water), were manifested and this affirmed the deterioration of coating layer in case of unmodified coating. EDX analysis for PA-DGEBA/MF coating was illustrated in Fig. 9b in which demonstrated more inhibited steel surface at count of 9.1 than in case of blank epoxy with appearance of Na and Cl^- ions in addition to presence of iron oxide moieties. Also, Fig. 9b manifested the presence of nitrogen atoms which affirmed the modification process with MF ligand. As shown in Fig. 9c, PA-DGEBA/bpy coated film offered more inhibited steel surface than that of PA-DGEBA/MF coating at count of 7.9 with appearance of Na and Cl^- ions in addition to presence of iron oxide moieties but with lower concentration than in case of PA-DGEBA/MF and neat epoxy coatings. Furthermore, Fig. 9c offered the presence of nitrogen atoms but with lower count than in case of PA-DGEBA/MF coated steel

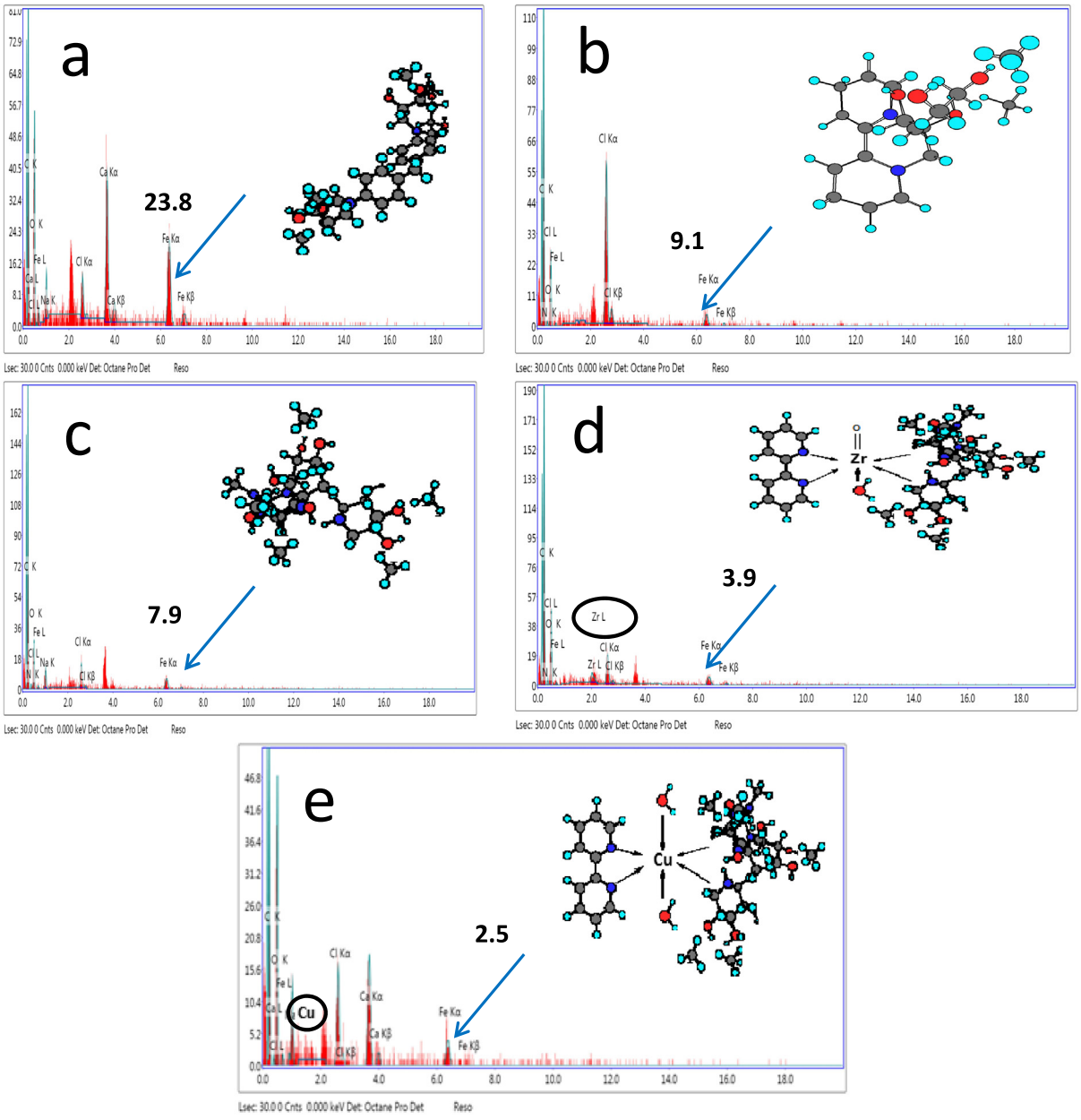

Fig. 9 EDX images of the investigated coated films a) Unmodified conventional epoxy, b) PA-DGEBA/MF, c) PA-DGEBA/bpy, d) PA-DGEBA/MC-Zr and e) PA-DGEBA/MC-Cu after the direct exposure to salt spray fog at severe conditions.

panel which affirmed the modification process with bpy ligand (less number of nitrogen atoms). PA-DGEBA/MC-Zr coating displayed an inhibited coating layer at count of 3.9 with appearance of very low concentration of chloride ions and rust than that of the modified coated films with free ligands as shown in Fig. 9d. Also, Fig. 9d showed the presence of Zr element with presence of nitrogen atoms which affirmed the modification process by Zr(IV) complex via the coating film. Finally, PA-DGEBA/MC-Cu coating offered a multi-protective behavior than the other investigated coated films in which offered the least iron count at 2.5 without appearance of rusting as shown in Fig. 9e. In addition, PA-DGEBA/MC-Cu coating displayed the presence of Cu metal with presence of nitrogen atoms which affirmed the modification process by Cu (II) complex via the coating layer.

The recognized results described the corrosion mitigation demeanor of the treated coated films with MF and bpy ligands affirmed that the enhanced cross-linking intensity in case of bpy than in case of MF with the excess of DGEBA (epoxy) moieties was responsible for the improved anti-corrosion behavior for PA-DGEBA/bpy coated panel than in case of PA-DGEBA/MF coating. For the modified coatings with Zr (IV) and Cu(II) mixed complexes, PA-DGEBA/MC-Cu coated panel showed the highest corrosion-inhibiting performance and this because Cu(II) complex had increased effective magnetic moment (μ_{eff}) at 1.70 M.B., but Zr(IV) complex offered diamagnetic properties. The increased magnetic moment value of Cu(II) mixed complex boosted the chemical interactions and affinity of binding between the active moieties of these molecules and the epoxy vehicle leading to reinforcing the density

of the cross-linking via coating film. This performance enhanced the steel/epoxy interfacial adhesion. The whole evaluation of the corrosion mitigation demeanor depended on the percent of polar bonds presented in the molecules. (Fadl et al., 2020; Fadl et al., 2019; El Ashry et al., 2006; Rochdi et al., 2014). Furthermore, PA-DGEBA/MC-Zr coated film displayed more efficient inhibitive leverage than PA-DGEBA/MF and PA-DGEBA/bpy coatings and this could be assigned to the highest atomic weight of Zr(IV)-complex than that of MF and bpy ligands (Eddy and Ita, 2011). The superb protective action for PA-DGEBA/MC-Cu coating could attributed to the full dispersion of Cu(II) mixed complex compounds with high μ_{eff} value through epoxy binder matrix as cross-linking modifiers in which prohibited the spreading of the corrosive salt spray fog species through the open channels of the cured coated layer by increasing the density of chemical bonding and forming an outstanding protective barrier.

The outstanding synergistic anti-corrosion demeanor of cured epoxy coating modified with MF, bpy and their investigated Zr(IV) and Cu(II) complexes on C-steel substrate of gas and oil production platforms and predominately, PA-DGEBA/MC-Cu coatings displayed the inhibitive mechanism illustrated in Fig. 10 and discussed as follows. The outstanding corrosion inhibiting action characterized by the presence of π- electrons of aromatic rings existed in epoxy resin and bpy ligands of the incorporated mixed complexes. In addition,

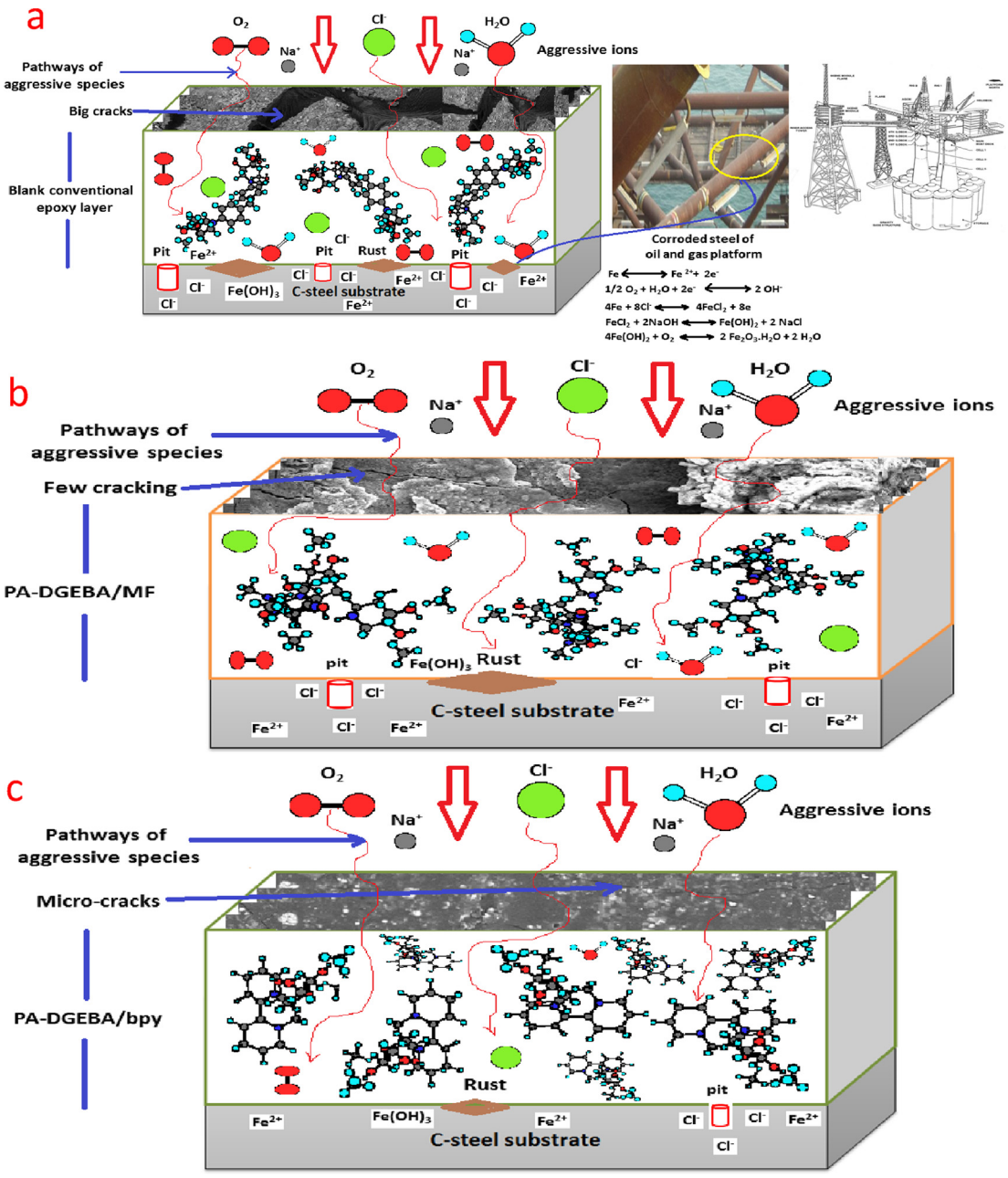

Fig. 10 The suggested anticorrosion mechanism of a) Polyamine cured conventional epoxy, b) PA-DGEBA/MF, c) PA-DGEBA/bpy, d) PA-DGEBA/MC-Zr and e) PA-DGEBA/MC-Cu, coated films.

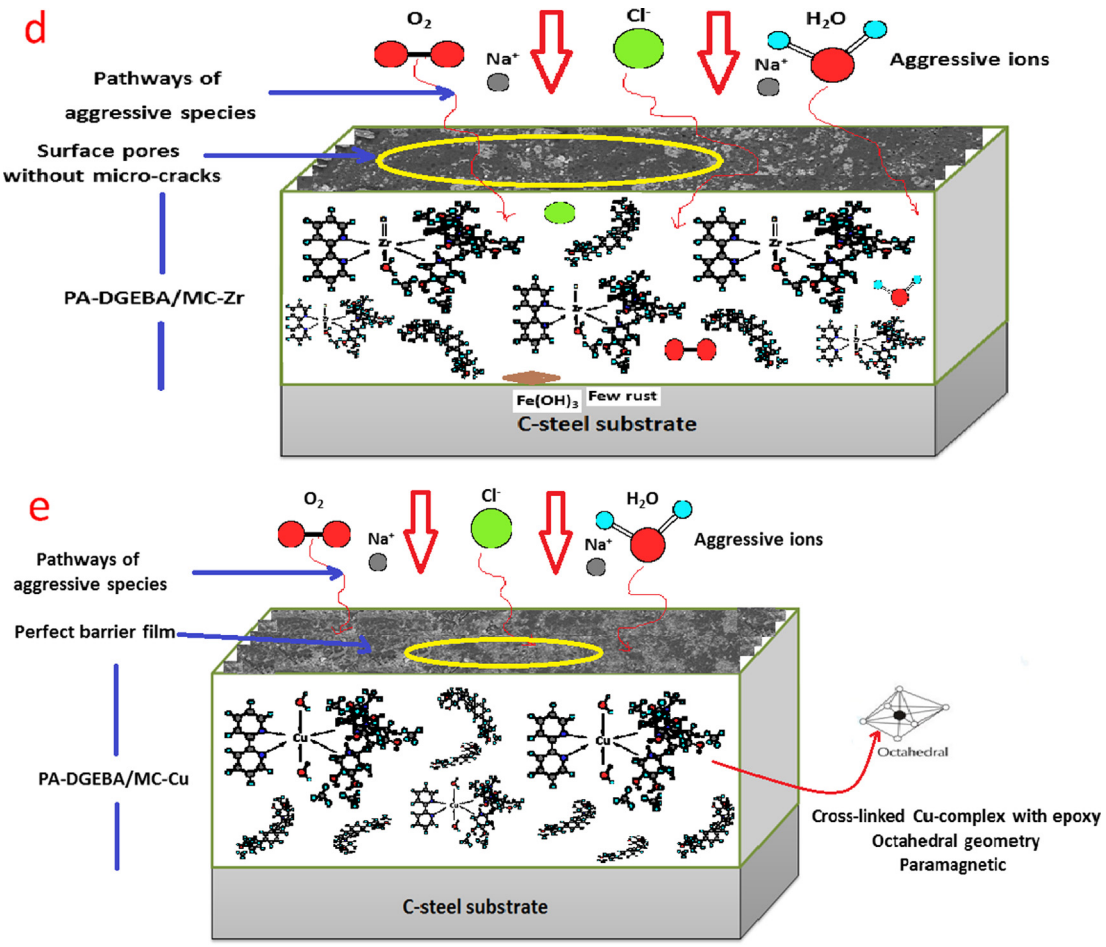

Fig. 10 (*continued*)

the adsorption of lone pair of electrons of nitrogen atoms existented in the imine (C = N) groups presented in MF and bpy ligands and lone pair of oxygen atoms existed in epoxy on the steel panel. As shown in Fig. 11, the chemical bonding between the vacant d-orbitals of steel surface and the donating centers of the coating layer established an adherent plastic film and this participate principally in the protective performance of these coatings. In addition, a strong electrostatic physical bonding could be induced between steel vacant sites and modified epoxy with MF, bpy and their mixed complexes and supported the protective behavior (Fadl et al., 2020). Fig. 11 offered a weak adherent plastic layer of cured unmodified epoxy. In case of PA-DGEBA/MF and PA-DGEBA/bpy coated films, the adhesion vehemence with steel surface was increased in presence of MF and bpy ligands due to enhancing the bonding intensity. Mild adhesion strength was presented by PA-DGEBA/MC-Zr coated layer as shown in Fig. 11 owing to the increasing in intensity of donor/acceptor interactions due to incorporating of Zr(IV) mixed complex containing MF and bpy ligands via epoxy vehicle. Due to the increase in bonding intensity, the diffusion of aggressive species through the open channels of the coating layer was prohibited more than in case of blank epoxy, PA-DGEBA/MF and PA-DGEBA/bpy coatings (Fadl et al., 2020; Fadl et al., 2019; Fadl et al., 2016). Very robust adherent layers were displayed by PA-DGEBA/MC-Cu coatings as shown in Fig. 11. According to the suggested anti-corrosion mechanism as shown in Fig. 10a, cured blank unmodified neat epoxy displayed a complete deteriorated coating layer due to the spreading of pores and big cracks as effective pathways over the coating layer in which the aggressive species (Cl^-, O_2 and H_2O) penetrated the surface pathways and caused pitting corrosion and formation of rust ($Fe(OH)_3$) (Ramezanzadeh et al., 2020; Elzaabalawy and Meguid, 2020; Li et al., 2019; Zhu et al., 2021). With incorporating of MF and bpy ligands via the coating film, the deterioration effect was decreased in which micro and few cracks were observed in addition to presence of some rusted areas and pitting corrosion by PA-DGEBA/MF and PA-DGEBA/bpy coatings, respectively. This demeanor was because of enhancing the cross-linking intensity by the combined effect of donating centers in epoxy vehicle and the employed ligands as illustrated in Fig. 10b and c. But, the investigated complexes offered lower energy gap *(ΔE)* value than free ligands and displayed higher chemical reactivity in addition to the increasing in their atomic weight, thereby reinforcing the density of cross-linking with epoxy moieties and enhancing the film stiffness. As shown in Fig. 10d, PA-DGEBA/MC-Zr coating demonstrated more inhibitive layer than in case of PA-DGEBA/MF and PA-DGEBA/bpy coatings in which few rust was observed without existence of pitting corrosion. This performance was owing to the full dispersion of diamagnetic Zr(IV) mixed complex with octahedral

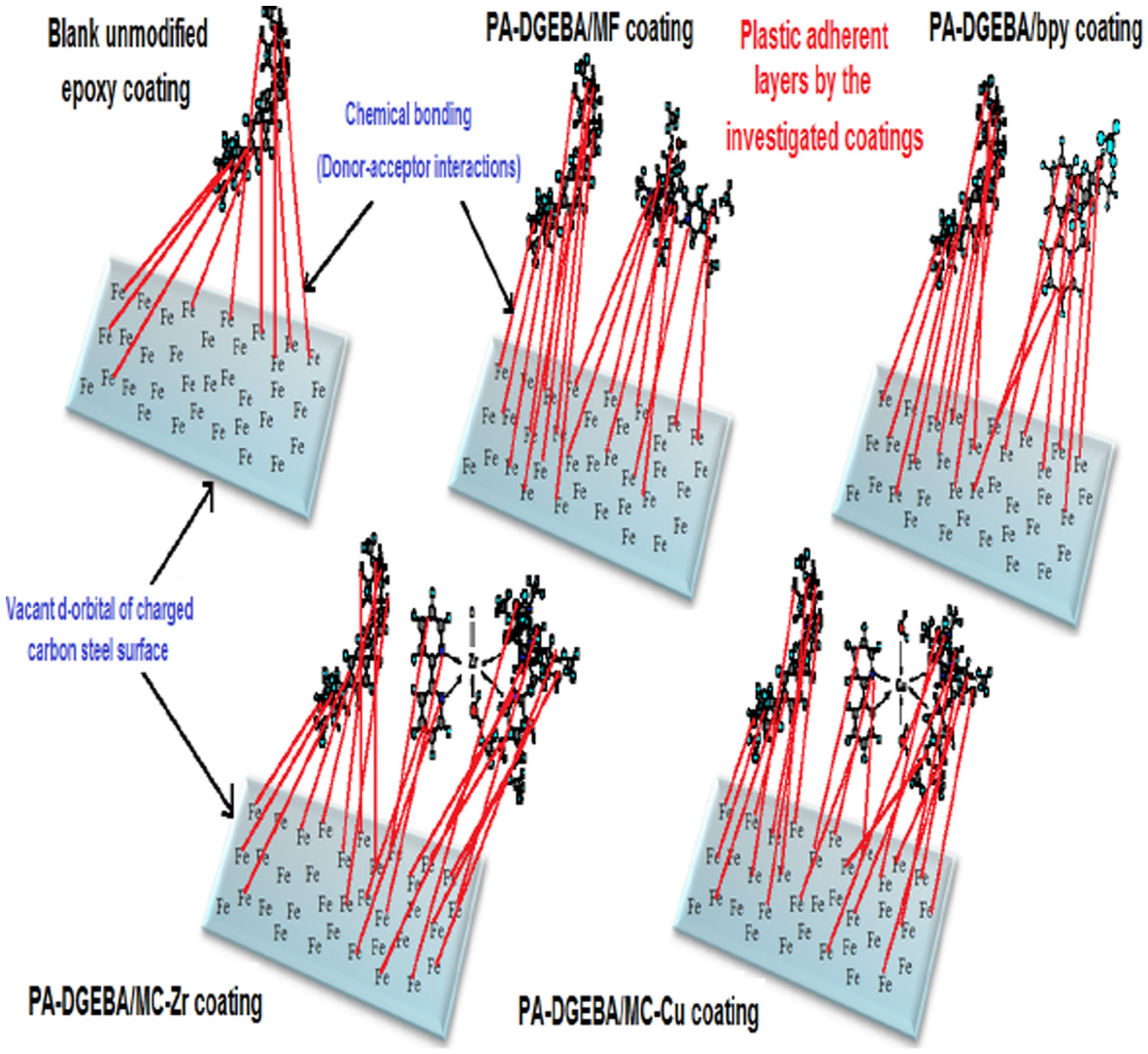

Fig. 11 Plastic adherent layers of the modified coated films against blank neat epoxy.

geometry and high molecular weight than in case of free ligands, thereby enhancing the cross-linking intensity, film rigidity and adhesion strength. Furthermore, the published literature affirmed that the magnetic moment and electronic spectral studies affected strongly in the inhibition performance of free metal complexes on the steel surface (Singh et al., 2013). The investigated results displayed that metal complexes with magnetic properties and octahedral structures offered more enhanced inhibition performance than that with diamagnetic ones. Fadl et al. investigated that metal complexes with paramagnetic properties demonstrated the prominent protective behavior via the epoxy coating film and the inhibitive effect was enhanced with increasing the effective magnetic moment value (Fadl et al., 2020; Fadl et al., 2019). The established barrier layer by PA-DGEBA/MC-Cu coating as displayed in Fig. 10e was assigned to the perfect dispersion of Cu(II) complex molecules with crystalline shape which arranged in overlapping sheets parallel to the C-steel substrate and established an enhanced interface surface interactions with epoxy, resulting in impervious shield and prohibited the permeation of corrosive ions, water and oxygen via the coating film. This performance consolidated the inter-coating adhesion and preventing coating layer swelling and cracking then, supported the corrosion inhibiting mechanism (Shi, 2009). PA-DGEBA/MC-Cu coating offered the outstanding protective performance because the Cu(II) mixed complex dispersed via the cured epoxy layer had paramagnetic properties (μ_{eff} = 1.70-M.B.) and an elongated octahedral molecular geometry. Also, the UV–Vis. spectra of MF, bpy and their metal complexes illustrated in Table 3 affirmed that Cu(II) mixed complex had π-π*, n-π* and d-d in addition to ligand–metal charge transfer transitions. These transitions could enhance the chemical bonding and density of cross-linking via coated film, thereby consolidating the epoxy layer hardness (Fadl et al., 2020) and preventing the penetration of aggressive species as shown in Fig. 10e. Furthermore, PA-DGEBA/MC-Cu coating offered a super-hydrophobic layer owing to enhancing the intensity of cross-linking between Cu(II) mixed complex and epoxy terminals. Then, the wettability of aggressive atmosphere was decreased (Fadl et al., 2019). However, Zr and Cu ions in case of Zr(IV) and Cu(II) complexes were chelated with the same ligands and also had the same molecular geom-

etry (octahedral), PA-DGEBA/MC-Zr displayed lower protective behavior than PA-DGEBA/MC-Cu. This behavior could be attributed to diamagnetic properties of Zr(IV) mixed complex with lower electronic transitions (Singh et al., 2013) as illustrated in Table 3. The dispersion of paramagnetic Cu(II) mixed complex with a distorted (elongated) octahedral structure geometry and had d-d transitions via the coating layer occupied the surface open zigzag channels as interconnected bridges with epoxy matrix and decreased the free volumes in addition to enhancing the density of cross-linking, thereby reducing segmental chain motions and reinforcing stiffness (Fadl et al., 2020; Liu et al., 2021).

3.8. Self-healing performance

The self-healing mechanism of PA-DGEBA/MC-Cu coating offered by checking the X-cutting zone over full-dried coated steel panel after the directly innuendo to the aggressive fog was illustrated in Fig. 12. The cured blank unmodified epoxy layer offered sfull electrolytic degradation at the surroundings of the cutting area as shown in Fig. 7 and illustrated in the mechanism shown in Fig. 10a and according to the equations (Schremp, 1984; Ramezanzadeh et al., 2019; Fadl et al., 2020; Ashassi-Sorkhabi et al., 2016; Gibson and Resins, 2017):

$$2Fe + O_2 + 4H^+ \rightarrow 2Fe^{2+} + 2H_2O \quad (3)$$

$$4Fe + 8Cl^- \rightarrow 4FeCl_2 + 8e' \quad (4)$$

$$4H_2O + 2O_2 + 8Na^+ + 8e' \rightarrow 8NaOH \quad (5)$$

$$FeCl_2 + 2NaOH \rightarrow Fe(OH)_2 + 2NaCl \quad (6)$$

$$4Fe(OH)_2 + O_2 \rightarrow 2Fe_2O_3{\bullet}\ H_2O + 2H_2O \quad (7)$$

But in case of PA-DGEBA/MC-Cu coating as shown in Fig. 12, the synergistic self-healing mechanism (autonomous) of MF-Cu-bpy complex as microcapsules and the excess of unreacted epoxy (DGEPA) moieties was appointed to the induced poly-condensation or cross-linking due to the innu-endo directly to truculent fog producing new cured phase over X-cut area from DGEPA-MF-Cu-bpy-DGEPA as consolidated deposits, prevented the migration of aggressive species (H_2O and ions) in the proximity of coating and inhibited the scratched zone (Fadl et al., 2020; Liu et al., 2021). Cu(II) complex with an elongated octahedral structure geometry offered self-healing performance owing to its enhanced electronegativity (χ) at −0.294 value and having the highest value of electron affinity (A) at −0.199, thereby supporting the chemical reaction with the un-reacted epoxy under the effect of external severe environment (salt spray aggressive fog), and boosting the intensity of cross-linking

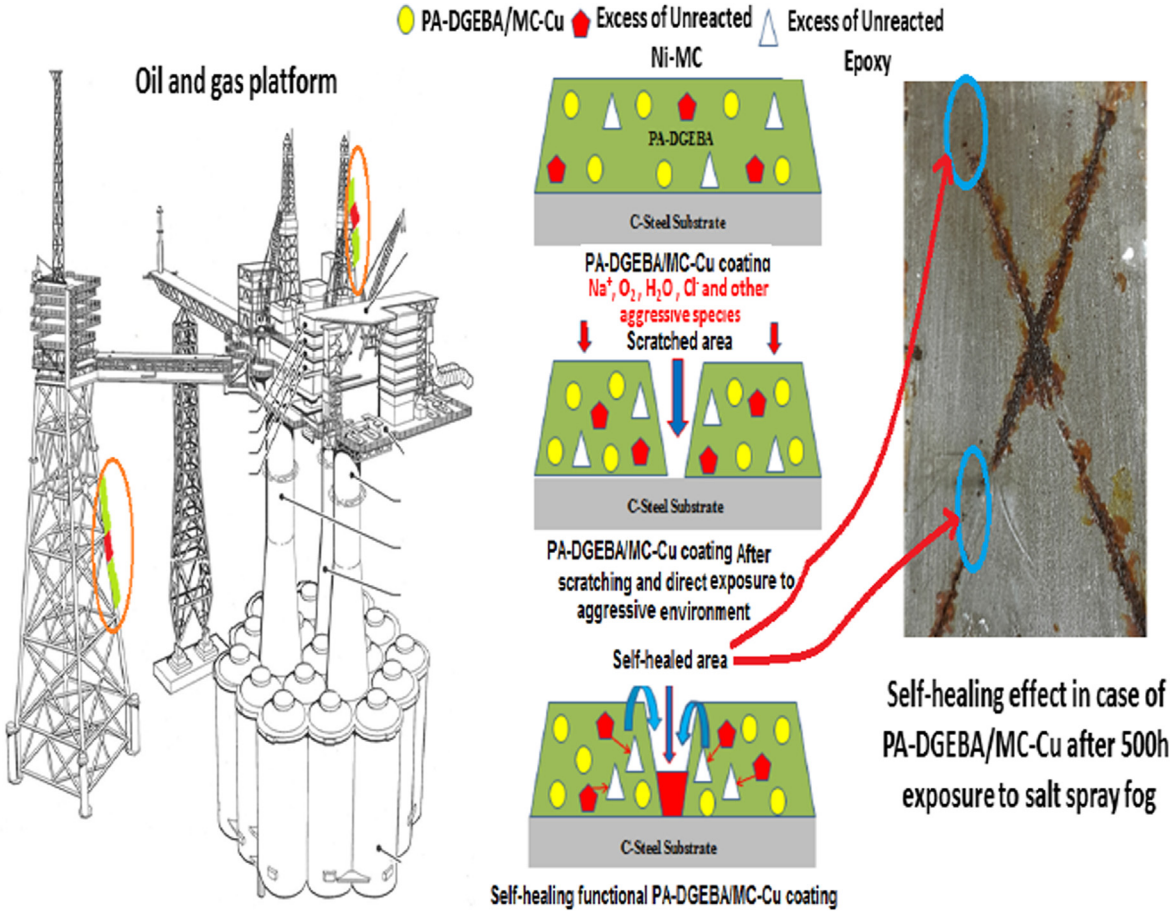

Fig. 12 Self-healing mechanism of PA-DGEBA/MC-Cu coating applied on the oil and gas platform.

over the uncoated area. Thereafter, the formed deposit adduct at the scratched zone self-healed on this area and mitigated the diffusion of aggressive species.

3.9. AFM analysis of the checked coated panels for protective behavior confirmation

The 3D AFM topographic images of the surveyed coatings (polynomial fits) after the direct exposure to the aggressive salt spray fog were illustrated with lateral dimensions of 100 × 100 nm as shown in Fig. 13. This strategy was performed to survey the protective performance of the employed modified coating with MF, bpy and their mixed complexes against the delamination effect of blank unmodified epoxy in 3D dimensions. The polynomial fits affirmed the corrosion inhibiting performance of modified coated panels especially, PA-DGEBA/MC-Zr and PA-DGEBA/MC-Cu coatings based on measuring the surface roughness and visual inspection of the formed rusting over the coating surface. Fig. 13a demonstrated ultra-microtomed fractured surface with some lamps, protuberances and degradation features over the coating surface with highly roughened surface (Ra = 1933 nm, Rq = 238 nm) due to the formation of corrosive products in case of blank neat epoxy (Gu et al., 2005). The surface modified MF coated film (PA-DGEBA/MF) offered also highly roughened surface (Ra = 176.7 nm, Rq = 27.4 nm) with observed protuberances but less than that observed in case of neat epoxy as displayed in Fig. 13b. PA-DGEBA/bpy

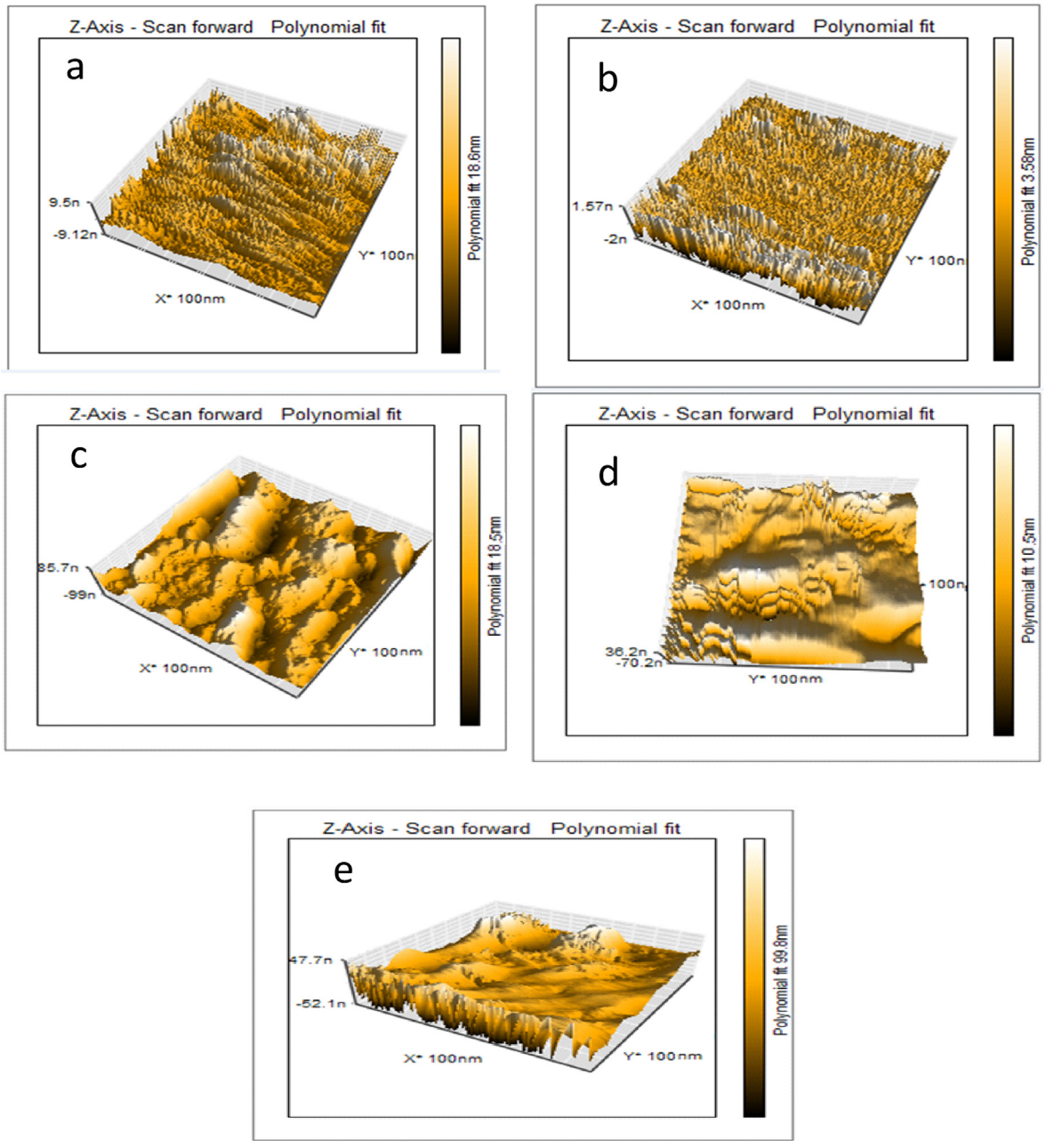

Fig. 13 3D AFM topographic images of the investigated coated films after the direct exposure to salt spray fog at severe conditions.

displayed low roughened coating surface with few protuberances (Ra = 9.46 nm, Rq = 11.28 nm) as shown in Fig. 13c due to the combined chemical bonding of cured bpy ligand and epoxy and enhancing the crosslinking intensity. The polynomial fit of PA-DGEBA/MC-Zr offered smoother surface with very small protuberances (Ra = 2.8 nm, Rq = 7.70 nm) as shown in Fig. 13d. This action was due to the presence of Zr(IV) mixed complex with octahedral molecular geometry and high atomic weight that enhanced the protective behavior in which enhanced the film rigidity and stiffness more than in case of free ligands. As displayed in Fig. 13e, PA-DGEBA/MC-Cu offered the most smooth surface (Ra = 1.78 nm, Rq = 2.99 nm) with a harder matrix of bulk microstructure of polyamine cured epoxy film modified with Cu(II) complex (nonporous layer). Also, This performance affirmed the self-healing effect of PA-DGEBA/MC-Cu coating after the long-term innuendo to the offensive fog for 21 days (500 h) in which the surface microstructure demonstrated un-damaged areas (Cui et al., 2019). The enhanced effective magnetic moment with an elongated octahedral geometry of Cu(II) mixed complex and the increased electronegativity were responsible for reinforcing the affinity of chemical binding and increasing the interface surface interactions with epoxy binder. Then after, it could promote the intensity of cross-linking via the internal coating and consolidate the steel/epoxy interfacial adhesion.

3.10. Acid spot resistance test of the checked coated steel specimens

The acid resistance test was implemented to offer the chemical degradation action of strong acids on the cured film of the checked PA-DGEBA/MF, PA-DGEBA/bpy, PA-DGEBA/MC-Zr and PA-DGEBA/MC-Cu coated films against blank unmodified epoxy. As shown in Fig. 14a and b and illustrated in Table 11, blank unmodified epoxy and PA-DGEBA/MF coatings displayed complete chemical failure (dense blistering, wrinkling, softening and surface damage) due to the direct

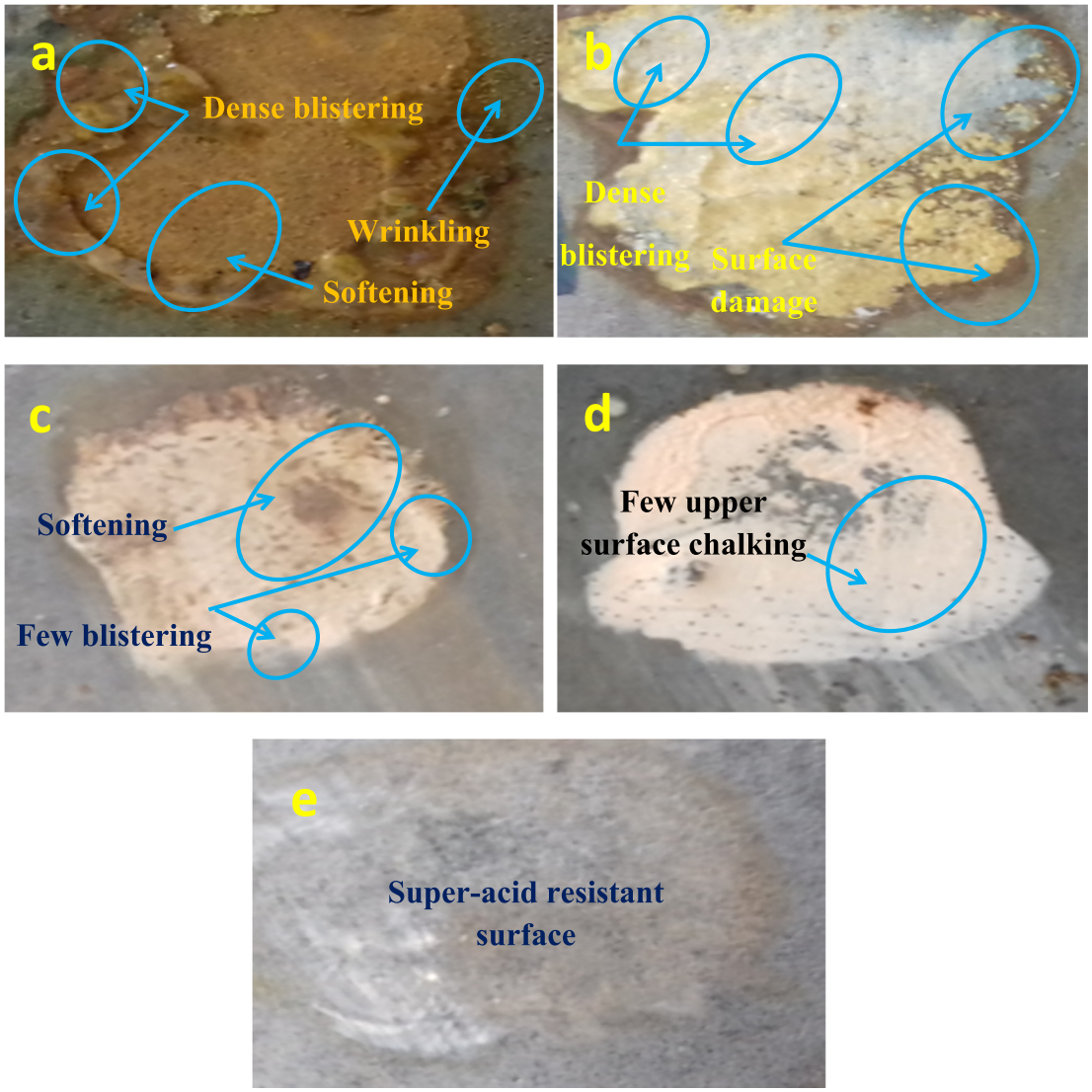

Fig. 14 Acid spot resistance test for the investigated coated films a) Unmodified conventional epoxy, b) PA-DGEBA/MF, c) PA-DGEBA/bpy, d) PA-DGEBA/MC-Zr and e) PA-DGEBA/MC-Cu.

Table 11 Acid spot test results for the investigated coatings.

Coating code	Acid resistance (B: Nonvolatile liquid)		
	Sulfuric acid (96%)	Nitric acid (70%)	Hydrochloric acid (37%)
Blank epoxy coating	3	3	3
PA-DGEBA/MF	2	2	1
PA-DGEBA/bpy	2	2	3
PA-DGEBA/MC-Zr	1	0	1
PA-DGEBA/MC-Cu	0	0	0

exposure to strong acids. This performance could be attributed to physical and chemical degradations in which the physical damage was due to the penetration of hydrolyzed moieties of acids via the free volumes of cured coating layer. Then, these polar moieties could "jump" from one free volume to another and caused blistering, wrinkling and softening. The chemical degradation of the coating layer was due to acid hydrolysis in addition to the initiated oxidation reactions occurred by the acid effect and caused coating bond fracturing and conversion of reactive groups (as –OH to –C = O) (Banna et al., 2011; George and Thomas, 2001; Abdou et al., 2019). Furthermore, H_2O molecules presented at the coating/steel interface could easily break the hydrogen bonds formed between the C-steel substrate and coating due to its strong affinity to establish strong hydrogen bond with steel. For water influence, the produced hydroxyl groups from the induced electrochemical reactions initiated underneath the coating film could react with Na^+ cations of tap water and form NaOH molecules as a strong alkaline agent. Thereafter, this demeanor increased the pH beneath the coating layer and caused delamination of coating (Sorenson et al., 2010). PA-DGEBA/bpy coating offered little chemical damage as displayed in Fig. 14c and illustrated in Table 11 due to the acid delamination effect. This behavior was due to the enhanced chemical bonding and highly cross-linking intensity by bpy ligand (single-double bond overlapping conjugated system) with epoxy matrix and formation of mild stable coating film. PA-DGEBA/MC-Zr coated layer showed more chemical resistance and few weak adherent spots as illustrated in Fig. 14d than for surface treated MF and bpy epoxy coatings due to the combined cross-linking of two ligands of Zr(IV) mixed complex with octahedral geometry and epoxy matrix which supported the donor/acceptor interface interactions with steel surface. The passed coatings displayed no softening; no loss of adhesion; no wrinkling and no blistering after the exposure period as sketched in Fig. 15. PA-DGEBA/MC-Cu coatings offered the superior acid resistance performance as shown in Fig. 14e and illustrated in Table 11.This behavior was due to the well-dispersion of the elongated octahedral structure of Cu(II) mixed complex which fill the free volume places via the coating film by inducing highly cross-linking intensity and worked as internal coating bridges, thereby decreasing segmental chain motions, enhancing the coating layer stiffness and ameliorating the resistance to acids effect (Marotta et al., 2021). In addition, PA-DGEBA/MC-Cu coating demonstrated the perfect chemical durability behavior due to the magnetic properties of Cu(II) mixed complex in which increased the electronegativity around the formed compound and enhanced the internal cross-linking with epoxy matrix. Then after, this performance could maximize the chemical bonding between the donor coating sites and vacant d-orbitals of steel substrate and boost the resistance to the external hazardous effect of various applied acids.

Finally, the proposed coating systems modified with the novel fabricated Cu(II) and Zr(IV) complexes as network crosslinking agents demonstrated new corrosion-inhibiting and chemical resistance properties. Their synergistic behaviors differed from commercially available anticorrosive agents owing to not only pigmentation and blocking the coating film open channels but also participation in enhancing the crosslinking intensity as extra curing agents for epoxy vehicle. This performance supported the donor/acceptor interactions via coating/steel interface and revealed a consolidated cured adherent film, thereby exhibiting an excellent durability against severe external exposures. Compared to the referenced articles investigated the traditional anticorrosive agents, it was observed that the present incorporated complexes performed as epoxy network interconnected bridges in which exhibited filling the free volumes via the epoxy network , reducing the segmental chain motion and supporting film stiffness.

4. Conclusions

Multi-functional epoxy coatings based on the modification by novel fabricated Cu(II) and Zr(IV) mixed complexes of MF and bpy ligands as coating intensive cross-linking accelerators were formulated and evaluated to manifest their anti-corrosion and chemical resistance properties applied on the steel surface of oil and gas production platforms. Several characterizations for the prepared complex cross-linkers were made and affirmed their chemical consistence. UV–Vis. spectra of the investigated compounds demonstrated that Cu(II) complex had π-π*, n-π*, LMCT and d-d transitions. The nodal properties of molecular orbitals of the complexes offered that Zr(IV) and Cu(II) complexes had lower energy gap ΔE values than free MF and bpy. So, these complexes demonstrated high reactivity than free ligands. The electronegativity (χ), and electron affinity (A) of these complexes achieved the highest values at –294 and –0.199, respectively and this affirmed the expected intensive cross-linking intensity could be established. PA-DGEBA/bpy coated film displayed proper corrosion-inhibiting and acid resistance properties

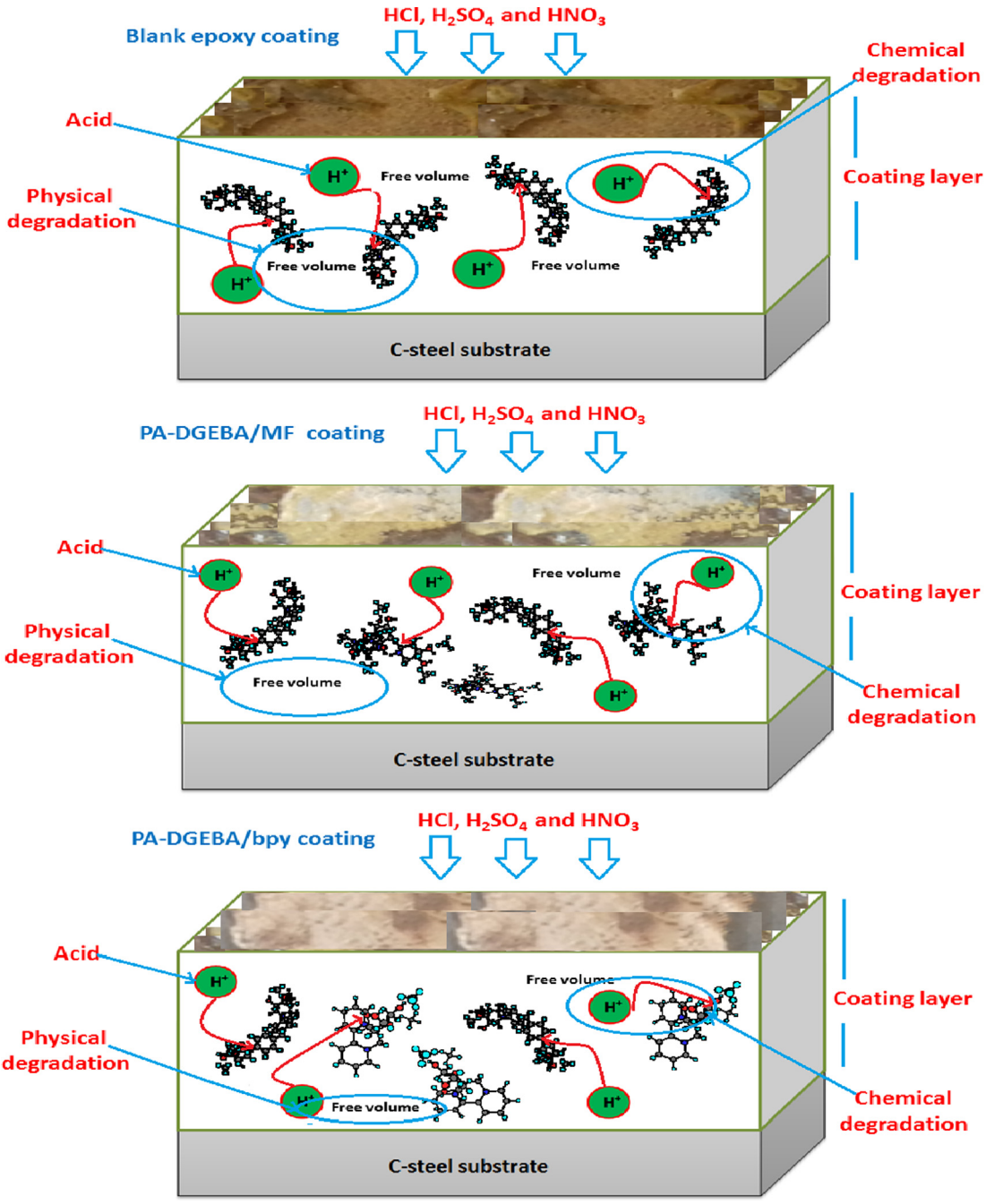

Fig. 15 Sketch for the predicted mechanism of acid resistances for the investigated coated films.

than PA-DGEBA/MF coating due to the enhanced cross-linking and formation of stable cured coating film by the reactive conjugated system of bpy with epoxy matrix. PA-DGEBA/MC-Zr coating demonstrated an enhancement in the resistance to outdoor exposures than PA-DGEBA/MF and PA-DGEBA/bpy coatings due to the dispersion of octahedral structured Zr(IV) complex with high atomic weight than in case of MF and bpy in which supported an elevated cross-linking density with epoxy. The prominent behavior was achieved by PA-DGEBA/MC-Cu coating owing to the synergistic effect by high effective dipole moment and an elongated octahedral molecular geometry, high electronegativity and electron affinity in addition to demonstrating four electronic transitions, thereby enhancing chemical bonding via donor/acceptor interactions between epoxy and steel surface and boosting the interfacial adhesion.

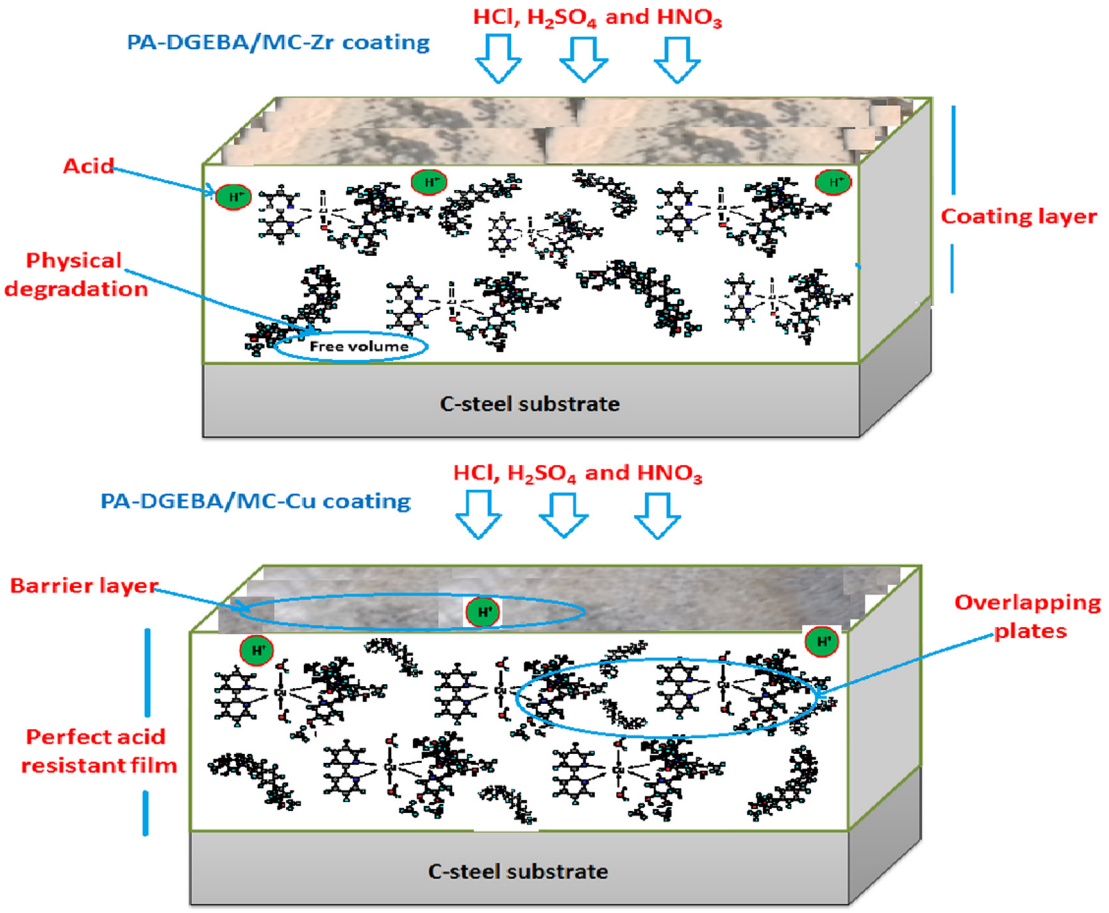

Fig. 15 (*continued*)

Declaration of Competing Interest

The authors declare that they have no known competing financial interests or personal relationships that could have appeared to influence the work reported in this paper.

Acknowledgment

Appreciation and gratitude submitted from authors to Egyptian Petroleum Research Institute and Zagazig University for the scientific and material assistance to produce this applied research study in the field of petroleum industry and materials engineering.

References

Olajire, A.A., 2017. Olajire, Corrosion inhibition of offshore oil and gas production facilities using organic compound inhibitors - A review. J. Mol. Liq. 248, 775–808.

https://www.pcimag.com/articles/105888-advanced-anti-corrosion-coating-utilized-on-two-north-sea-offshore-platforms, (2019).

Schremp, F.W., 1984. Corrosion Prevention for Offshore Platforms. J. Pet. Technol. 36, 605–612.

Ramezanzadeh, B., Karimi, B., Ramezanzadeh, M., Rostami, M., 2019. Synthesis and characterization of polyaniline tailored graphene oxide quantum dot as an advance and highly crystalline carbon-based luminescent nanomaterial for fabrication of an effective anti-corrosion epoxy system on mild steel. J. Taiwan Inst. Chem. Eng. 95, 369–382.

Fadl, A.M., Abdou, M.I., Hamza, M.A., Sadeek, S.A., 2020. Corrosion-inhibiting, self-healing, mechanical-resistant, chemically and UV stable PDMAS/TiO2 epoxy hybrid nanocomposite coating for steel petroleum tanker trucks. Prog. Org. Coat. 146, 105715.

Ashassi-Sorkhabi, H., Seifzadeh, D., Raghibi-Boroujeni, M., 2016. Analysis of electrochemical noise data in both time and frequency domains to evaluate the effect of ZnO nanopowder addition on the corrosion protection performance of epoxy coatings. Arab. J. Chem. 9, S1320–S1327.

G. Gibson, Epoxy Resins, in: Brydson's Plast. Mater. Eighth Ed., 2017: pp. 773–797.

Yue, S.u., 2020. Shi hui Qiu, Dongping Yang, Shuan Liu, Haichao Zhao, Liping Wang, Qunji Xue, Active anti-corrosion of epoxy coating by nitrite ions intercalated MgAl LDH. J. Hazard. Mater. 391, 122215.

Pourhashem, S., Vaezi, M.R., Rashidi, A., Bagherzadeh, M.R., 2017. Exploring corrosion protection properties of solvent based epoxy-graphene oxide nanocomposite coatings on mild steel. Corros. Sci. 115, 78–92.

Qiu, S., Chen, C., Zheng, W., Li, W., Zhao, H., Wang, L., 2017. Long-term corrosion protection of mild steel by epoxy coating containing self-doped polyaniline nanofiber. Synth. Met. 229, 39–46.

Pourhashem, S., Vaezi, M.R., Rashidi, A., 2017. Investigating the effect of SiO2-graphene oxide hybrid as inorganic nanofiller on corrosion protection properties of epoxy coatings. Surf. Coat. Technol. 311, 282–294.

Ganjaee, M., Ramezanzadeh, B., 2020. Epoxy composite coating corrosion protection properties reinforcement through the addition

of hydroxyl-terminated hyperbranched polyamide non-covalently assembled graphene oxide platforms. Constr. Build. Mater. 234, 117421.
P. Vasantha, B. Sathish Kumar, B. Shekhar, P.V. Anantha Lakshmi, Cobalt(II)–metformin complexes containing α-diimine/α-diamine as auxiliary ligand: DNA binding properties, Appl. Organomet. Chem. 32 (2018) e4074.
Shahabadi, N., Heidari, L., 2012. Binding studies of the antidiabetic drug, metformin to calf thymus DNA using multispectroscopic methods. Spectrochim. Acta A 97, 406–410.
Mahmoud, M.A., Abdel-Salam, E.T., Abdel Aal, N.F., Showery, Z. M., Sallam, S.A., 2019. Dy(III) complexes of metformin Schiff-bases as glucose probe: synthesis, spectral, and thermal properties. J. Coord. Chem. 72, 1–20.
El-Shwiniy, W.H., Abbass, L.M., Sadeek, S.A., Zordok, W.A., 2020. Synthesis, Structure, and Biological Activity of Some Transition Metal Complexes with the Mixed Ligand of Metformin and 1,4-Diacetylbenzene. Russ. J. Gen. Chem. 90 (3), 483–488.
Zhu, M., Lu, L., Yang, P., Jin, X., 2002. Bis (1,1-dimethylbiguanido) copper(II) octahydrate. Acta Cryst. E 58, 217–219.
Schubert, U.S., Eschbaumer, C., 2002. Macromolecules Containing Bipyridine and Terpyridine Metal Complexes: Towards Metallo-supramolecular Polymers. Angew. Chem. Int. Ed. 41, 2892–2926.
Kaes, C., Katz, A., Hosseini, M.W., 2000. Bipyridine: the most widely used ligand. A review of molecules comprising at least two 2,2'-bipyridine units. Chem. Rev. 100, 3553–3590.
Elsevier, C.J., Reedijk, J., Walton, P.H., Ward, M.D., 2003. Ligand design in coordination chemistry: approaches to new catalysts, new materials, and a more sustainable environment. Dalton Trans. 10, 1869–1880.
Igor V. Solovyev, Aleksandar Kondinski, Kirill Yu. Monakhov, Igor O. Koshevoy Elena V. Grachova , Synthesis, photophysical properties and cation-binding studies of bipyridine-functionalized gold (i) complexes, Inorg. Chem. Front. 5 (2018) 160-171.
Abd El-Hamid, S.M., El-Demerdash, R.S., Arafat, H.F.H., Sadeek, S. A., 2017. Spectroscopic studies and thermal analysis of mononuclear metal complexes with moxifloxacin and 2,2′-bipyridine and their effects on acute lung injury induced by hydrochloric. J. Mol. Struct. 1149, 613–625.
Dendrinou-Samara, C., Psomas, G., Raptopoulou, C.P., Kessissoglou, D.P., 2001. Copper (II) complexes with phenoxyalkanoic acids and nitrogen donor heterocyclic ligands: structure and bioactivity. J. Inorg. Biochem. 83, 7–16.
Efthimiadou, E.K., Katsaros, N., Karaliota, A., Psomas, G., 2007. Mononuclear copper (II) complexes with quinolones and nitrogen-donor heterocyclic ligands: Synthesis, characterization, biological activity and interaction with DNA. Inorg. Chim. Acta 360, 4093–4102.
A.M. Fadl, M.I. Abdou, Doaa Laila, S.A. Sadeek, Fabrication and characterization of novel p-Phenylamine-N(4-chloro salicylaldenemine) ligand and its metal complexes and evaluation their anti-corrosion and chemical resistance properties in epoxy/SiO2 nanocomposite for steel surface coating, Chem. Eng. J. 384 (2020) 123390.
A.M. Fadl, M.I. Abdou, Doaa Laila, S.A. Sadeek, Application insights of Schiff base metal complex/SiO2 hybrid epoxy nanocomposite for steel surface coating: corre-lation the protective behavior and mechanical properties with material loading, Prog. Org. Coat. 136 (2019) 105226.
Zhang, Wenyuan, Zhang, Wenchao, Pan, Ye-Tang, Yang, Rongjie, 2021. Facile synthesis of transition metal containing polyhedral oligomeric silsesquioxane complexes with mesoporous structures and their applications in reducing fire hazards, enhancing mechanical and dielectric properties of epoxy composites. J. Hazard. Mater. 401, 123439.
Ramanathan S. Lalgudi, Barry L. Mcgraw, Robert J. Cain, Metal complexes used as driers in coatings, A patent no. WO2009134508A2, 2009.
Harrington, M.J., Masic, A., Holten-Andersen, N., Waite, J.H., Fratzl, P., 2010. Iron-clad fibers: a metal-based biological strategy for hard flexible coatings. Science 328, 216–220.
Ejima, H., Richardson, J.J., Liang, K., Best, J.P., van Koeverden, M. P., Such, G.K., Cui, J., Caruso, F., 2013. One-step assembly of coordination complexes for versatile film and particle engineering. Science 341 (6142), 154–157.
Li, L., Zhang, G., Su, Z., 2016. The most popular pair of orthogonal dynamic bonds, hydrazones 2 and disulfides 3. Angew. Chem. 128, 9239–9242.
Yan, Ru, Gao, Xiang, He, Wei, Guo, Rui, Wu, Ruonan, Zhao, Zhuangzhi, Ma, Houyi, 2017. A simple and convenient method to fabricate new types of phytic acid–metal conversion coatings with excellent anti-corrosion performance on the iron substrate. RSC Adv. 7 (65), 41152–41162.
Frisch, M.J. et al, 1998. Gaussian 98, Revision A.6 Inc. Pittsburgh PA.
Kohn, W., Sham, L.J., 1965. Self-Consistent Equations Including Exchange and Correlation Effects. Phys. Rev. A 140, 1133.
Becke, A.D., 1988. Density-functional exchange-energy approximation with correct asymptotic behavior. Phys. Rev. A 38, 3098.
Lee, C., Yang, W., Parr, R.G., 1988. Development of the Colle-Salvetti correlation-energy formula into a functional of the electron density. Phys. Rev. B. 37, 785.
R.L. Flurry Jr., Molecular Orbital Theory of Bonding in Organic Molecules, Marcel Dekker, New York, 1968.
ASTM D1308 - 02e: Standard Test Method for Effect of Household Chemicals on Clear and Pigmented Organic Finishes, STM International, West Conshohocken, PA, 2002.
Geary, W.J., 1971. The Use of Conductivity Measurements in Organic Solvents for the Characterization of Coordination Compounds. Coord. Chem. Rev. 7, 81–122.
Deacon, G.B., Phillips, R.J., 1980. Relationships between the carbon-oxygen stretching frequencies of carboxylato complexes and the type of carboxylate coordination. Coord. Chem. Rev. 33, 227–250.
Magdy Shebl, M. Saif, Asmaa I. Nabeel and R. Shokry, New non-toxic transition metal nanocomplexes and Zn complex-silica xerogel nanohybrid: Synthesis, spectral studies, antibacterial, and antitumor activities, J. Mol. Str. 1118 (2016) 335-343.
Shahabadi, N., Heidari, L., 2014. Synthesis, Characterization and multi-spectroscopic DNA interaction studies of a new platinum complex containing the drug metformin. Spectrochim. Acta A. 128, 377–385.
Vasantha, P., Kumar, B.S., Shekhar, B., Lakshmi, P.V.A., 2018. Copper-metformin ternary complexes: Thermal, photochemosensitivity and molecular docking studies. Mater. Sci. Eng., C 90, 621–633.
Olar, Rodica, Badea, M., Cristurean, E., Lazar, V., Cernat, R., Balotescu, C., 2005. Thermal behavior, spectroscopic and biological characterization of Co (II), Zn (II), Pd (II) and Pt (II) complexes with N, N-dimethylbiguanide. J. Therm. Anal. Calorim. 80 (2), 451–455.
Al-Qadsy, Inas, 2020. Waseem Sharaf Saeed, Abdel-Basit Al-Odayni, Lena Ahmed Saleh Al-Faqeeh, Abdulaziz Ali Alghamdi, Mazahar Farooqui. Materials (Basel). 13, 514.
Olar, Rodica, Badea, Mihaela, Marinescu, Dana, Chifiriuc, Mariana-Carmen, Bleotu, Coralia, Grecu, Maria Nicoleta, Iorgulescu, Emilia-Elena, Lazar, Veronica, 2010. N, N-dimethylbiguanide complexes displaying low cytotoxicity as potential large spectrum antimicrobial agents. Eur. J. Med. Chem. 45 (7), 3027–3034.
El-Shwiniy, Walaa H., Gamil, Manar A., Sadeek, Sadeek A., Zordok, Wael A., El-farargy, Ahmed F., 2020. Ligational, DFT modeling and biological properties of some new metal complexes with 3-(bromoacetyl)coumarin and 1,10-phenanthroline. Appl. Orgmetal. Chem. 34 (8). https://doi.org/10.1002/aoc.v34.810.1002/aoc.5696.
Sadeek, S.A., Abd El-Hamid, S.M., Mohamed, A.A., Zordok, W.A., El-Sayed, H.A., 2019. Spectroscopic characterization, thermogravimetry, density functional theory and biological studies of some mixed-ligand complexes of meloxicam and 2,2′-bipyridine with some transition metals. Appl. Organomet. Chem. 33, 4889.

Abd El-Hamid, Sherif M., Sadeek, Sadeek A., Zordok, Wael A., El-Shwiniy, Walaa H., 2019. Synthesis, spectroscopic studies, DFT calculations, cytotoxicity and antimicrobial activity of some metal complexes with ofloxacin and 2, 2′-bipyridine. J. Mol. Struct. 1176, 422–433.

Refat, Moamen S., Al-Azab, Fathi M., Al-Maydama, Hussein M.A., Amin, Ragab R., Jamil, Yasmin M.S., Kobeasy, Mohamed I., 2015. Synthesis, spectroscopic and antimicrobial studies of La (III), Ce (III), Sm (III) and Y (III) Metformin HCl chelates. Spectrochim. Acta. A Mol Biomol. Spect. 142, 392–404.

Sadeek A. Sadeek, Sherif M. Abd El-Hamid, Walaa H. El-Shwiniy, Synthesis, spectroscopic characterization, thermal stability and biological studies of mixed ligand complexes of gemifloxacin drug and 2,2′-bipyridine with some transition metals, Res. Chem. Intermed. 42 (2016) 3183–3208.

Hayashi, Yukiko, Kita, Shouichi, Brunschwig, Bruce S., Fujita, Etsuko, 2003. Involvement of a Binuclear Species with the Re−C(O)O−Re Moiety in CO2 Reduction Catalyzed by Tricarbonyl Rhenium(I) Complexes with Diimine Ligands: Strikingly Slow Formation of the Re−Re and Re−C(O)O−Re Species from Re(dmb)(CO)3S (dmb = 4,4‘-Dimethyl-2,2‘-bipyridine, S = Solvent). J. Am. Chem. Soc. 125, 11976–11987.

Sadeek, Sadeek Atia, El-Attar, Mohamed Saed, Abd El-Hamid, Sherif Mohamed, 2015. Complexes and Chelates of Some Bivalent and Trivalent Metals with Ciprofloxacin Schiff Base. Synth. React. Inorg. Metal-Org Nano-Metal Chem. 45 (9), 1412–1426.

Sadeek, S.A., El-Attar, M.S., Abd El-Hamid, S.M., 2015. Synthesis and characterization and antibacterial activity of some new transition metal complexes with ciprofloxacin-imine. Bull. Chem. Soc. Ethlop. 29 (2), 259. https://doi.org/10.4314/bcse.v29i2.9.

Sadeek, Sadeek A., 2005. Synthesis, thermogravimetric analysis, infrared, electronic and mass spectra of Mn (II), Co (II) and Fe (III) norfloxacin complexes. J. Mol. Struct. 753 (1-3), 1–12.

Defazio, S., Cini, R., 2002. Synthesis, X-ray structure and molecular modelling analysis of cobalt(ii), nickel(ii), zinc(ii) and cadmium(ii) complexes of the widely used anti-inflammatory drug meloxicam. J. Chem. Soc., Dalton Trans. 22, 1888–1897.

Coats, A.W., Redfern, J.P., 1964. Kinetic Parameters from Thermogravimetric Data. Nature 201 (4914), 68–69.

Horowitz, H.H., Metzger, Gershon, 1963. A New Analysis of Thermogravimetric Traces. Anal. Chem. 35 (10), 1464–1468.

Moore, J.W., Pearson, R.G., 1981. Kinetics and Mechanism. John Wiley, New York.

Omar, M.M., 2009. Spectral, thermal and biological activity studies on Ruthenium(II) complexes with some pyridylamines. J. Therm. Anal. Calorim. 96 (2), 607–615.

Rotaru, A., Goşa, M., Rotaru, P., 2008. Computational thermal and kinetic analysis. J. Therm. Anal. Calorim. 94 (2), 367–371.

Mahmoud, W.H., Mohamed, G.G., El-Dessouky, M.M.I., 2014. Coordination modes of bidentate lornoxicam drug with some transition metal ions. Synthesis, characterization and in vitro antimicrobial and antibreastic cancer activity studies. Spectrochim. Acta A 122, 598–608.

Abd El-Hamid, Sherif M., Sadeek, Sadeek A., Zordok, Wael A., El-Shwiniy, Walaa H., 2019. Synthesis, spectroscopic studies, DFT calculations, cytotoxicity and antimicrobial activity of some metal complexes with ofloxacin and 2,2\-bipyridine. J. Mol. Struct. 1176, 422–433.

Deghadi, Reem G., Mahmoud, Walaa H., Mohamed, Gehad G., 2020. Metal complexes of tetradentate azo-dye ligand derived from 4,4’-oxydianiline; Preparation, structural investigation, biological evaluation and MOE studies. Appl. Organometal. Chem. 34 (10). https://doi.org/10.1002/aoc.v34.1010.1002/aoc.5883.

Yan, Lei, Wang, Xiaoyang, Zhou, Meisu, 2016. Synthesis, structural characterization and catalytic properties of a N-functionalized organoamide zirconium complex. Inorg. Chem. Commun. 65, 32–34.

Khandar, A.A., Azar, Z.M., Eskandani, M., Hubschle, C.B., Smaalen, S., Shaabani, B., Omidi, Y., 2019. Cadmium (II) complexes of a hydrazone ligand: Synthesis, characterization DNA binding, cyto- and genotoxicity studies. Polyhedron 171, 237–248.

Fleming, I., 1976. Frontier Orbitals and Organic Chemical Reactions. Wiley, London.

Kurtaran, R., Odabasoglu, S., Azizoglu, A., Kara, H., Atakol, O., 2007. Experimental and computational study on [2, 6-bis 3, 5-dimethyl-N-pyrazolyl) pyridine]-(dithiocyanato) mercury (II). Polyhedron 26, 5069–5074.

M. Abd El-Hamid, S., A. Sadeek, S., A. Zordok, W., G. Rashid, N., 2020. Spectroscopic properties, molecular structure, anticancer and antimicrobial evaluation of some new moxifloxacin metal complexes in the presence of 1,10-phenanthroline. Bull. Chem. Soc. Ethiop. 34 (2), 295–312.

Wahba, O.A.G., Hassan, A.M., Naser, A.M., Hanafi, A.M., 2017. Preparation and spectroscopic studies of some copper and nickel schiff base complexes and their applications as colouring pigments in protective paints industry. Egypt. J. Chem. 60, 25–40.

Abdou, M.I., Ayad, M.I., Diab, A.S.M., Hassan, I.A., Fadl, A.M., 2017. Influence of surface modified ilmenite/melamine formaldehyde composite on the anti-corrosion and mechanical properties of conventional polyamine cured epoxy for internal coating of gas and oil transmission pipelines. Prog. Org. Coat. 113, 1–14.

Depoorter, Nicolas, Coutellier, Daniel, Mužic, Markus, Berg-Pollack, Antje, Cai, Ye, Zimmermann, Andre, 2006. Damage evolution in a filled epoxy resin. Acta Mater. 54 (4), 927–934.

Abdou, M.I., Fadl, A.M., 2019. Assessment of nano-$FeTiO_3$/non crystalline silica cold galvanizing composite coating as a duplex corrosion guard system for steel electricity transmission towers in severe aggressive media. Constr. Build. Mater. 223, 705–723.

El Ashry, E.S.H., El Nemr, A., Esawy, S.A., Ragab, S., 2006. Corrosion inhibitors Part II: Quantum chemical studies on the corrosion inhibitions of steel in acidic medium by some triazole, oxadiazole and thiadiazole derivatives. Electrochim. Acta 51, 3957–3968.

Rochdi, A., Kassou, O., Dkhireche, N., Touir, R., El Bakri, M., Ebn Touhami, M., Sfaira, M., Mernari, B., Hammouti, B., 2014. Inhibitive properties of 2,5-bis (n-methylphenyl)-1,3,4-oxadiazole and biocide on corrosion, biocorrosion and scaling controls of brass in simulated cooling water. Corros. Sci. 80, 442–452.

Eddy, Nnabuk O., Ita, Benedict I., 2011. QSAR, DFT and quantum chemical studies on the inhibition potentials of some carbozones for the corrosion of mild steel in HCl. J. Mol. Model. 17 (2), 359–376.

A.M. Fadl, A.M. Al-Sabagh, M.I. Abdou, M.A. Migahed, Method for preparation epoxy lotion from ilmenite ore to protect steel structures from corrosion, ARE Patent no. 27679, 2016.

Ramezanzadeh, Mohammad, Ramezanzadeh, Bahram, Sari, Morteza Ganjaee, Saeb, Mohammad Reza, 2020. Morteza Ganjaee Sari, Mohammad Reza Saeb, Corrosion resistance of epoxy coating on mild steel through polyamidoamine dendrimer-covalently functionalized graphene oxide nanosheets. J. Ind. Eng. Chem. 82, 290–302.

Elzaabalawy, Assem, Meguid, Shaker A., 2020. Development of novel superhydrophobic coatings using siloxane-modified epoxy nanocomposites. Chem. Eng. J. 398, 125403.

Li, Mengyu, Liu, Ning, Chen, Jinhang, Li, Qiaoling, 2019. Simple construction based on epoxy-bonded super-hydrophobic anti-corrosion coating. J. Taiwan Inst. Chem. Eng. 95, 682–691.

Xiaobo Zhu, Haichao Zhao, Liping Wang, Qunji Xue, Bioinspired Ultrathin Graphene Nanosheets Sandwiched Between Epoxy Layers for High Performance of Anticorrosion Coatings, Chem. Eng. J. In press, Corrected Proof, (2020) 128301.

Singh, Pooja, Singh, Ashish K., Singh, Vinod P., 2013. Synthesis, structural and corrosion inhibition properties of some transition metal(II) complexes with *o*-hydroxyacetophenone-2-thiophenoyl hydrazone. Polyhedron 65, 73–81.

Shi, Xianming, 2009. Taun Anh Nguyen, Zhiyong Suo, Yajun Liu, Recep Avci, Effect of nanoparticles on the anticorrosion and mechanical properties of the epoxy coating. Surf. Coat. Technol. 204, 237–245.

Liu, Tengfei, Li, Wen, Zhang, Chenyang, Wang, Wei, Dou, Wenwen, Chen, Shougang, 2021. Preparation of highly efficient self-healing anticorrosion epoxy coating by integration of benzotriazole corrosion inhibitor loaded 2D-COF. J. Ind. Eng. Chem. 97, 560–573.

Xiaohong Gu, Tinh Nguyen, Mounira Oudina, David Martin, Bouchra Kidah, Joan Jasmin, Aziz Rezig, Lipiin Sung, Eric Byrd, Jonathan W. Martin, Derek L. Ho, Y. C. Jean, Microstructure and morphology of amine-cured epoxy coatings before and after outdoor exposures—An AFM study, J Coat. Technol. Res. 2 (2005) 547.

Cui, Jun, Li, Xiuqing, Pei, Zhiqiang, Pei, Yuansheng, 2019. A long-term stable and environmental friendly self-healing coating with polyaniline/sodium alginate microcapsule structure for corrosion protection of water-delivery pipelines. Chem. Eng. J. 358, 379–388.

Banna, M.H., Shiroko, J., Molgaard, J., 2011. Effects of two aqueous acidic solutions on polyester and bisphenol A epoxy vinyl ester resins. Mater. Sci. Eng., A 528, 2137–2142.

George, Soney C, Thomas, Sabu, 2001. Transport phenomena through polymeric systems. Prog. Poly. Sci. 26 (6), 985–1017.

Abdou, M.I., Ayad, M.I., Diab, A.S.M., Hassan, I.A., Fadl, A.M., 2019. Studying the corrosion mitigation behavior and chemical durability of FeTiO3/melamine formaldehyde epoxy composite coating for steel internal lining applications. Prog. Org. Coat. 133, 325–339.

Sorenson, P.A., Dam-Johansen, K., Weinell, C.E., Kiil, S., 2010. Cathodic delamination: quantification of ionic transport rates along coating-steel interfaces. Prog. Org. Coat. 67, 107–115.

Marotta, Angela, Faggio, Noemi, Ambrogi, Veronica, Mija, Alice, Gentile, Gennaro, Cerruti, Pierfrancesco, 2021. Biobased furan-based epoxy/TiO2 nanocomposites for the preparation of coatings with improved chemical resistance. Chem. Eng. J. 406, 127107.